Pervasive fitness trade-offs revealed by rapid adaption in large experimental populations of *Drosophila melanogaster*

M.C. Bitter*[1], S. Greenblum*[1,2], S. Rajpurohit*[3,4], A.O. Bergland[1,5], J.A. Hemker[1], N.J. Betancourt[3], S. Tilk[1], S. Berardi[3], H. Oken, P. Schmidt[+3], and D.A. Petrov[+1,6]

1 – Department of Biology, Stanford University, Stanford, CA, USA
2 – DOE Joint Genome Institute, Lawrence Berkeley National Laboratory, Berkeley, CA, USA
3 – Department of Biology, University of Pennsylvania, Philadelphia, PA, USA
4 – Division of Biological and Life Sciences, School of Arts and Sciences, Ahmedabad University, Gujarat, India
5 – Department of Biology, University of Virginia, Charlottesville, VA, USA
6 – Chan Zuckerberg Biohub, San Francisco, CA, USA

* equal contribution
[+] equal contribution

Corresponding authors: M.C.B (mcbitter@stanford.edu), P.S. (schmidtp@upenn.edu), and D.A.P (dpetrov@stanford.edu)

Abstract

Life-history trade-offs are an inherent feature of organismal biology that evolutionary theory posits play a key role in patterns of divergence within and between species. Efforts to quantify trade-offs are largely confined to phenotypic measurements and the identification of negative genetic-correlations among fitness-relevant traits. Here, we use time-series genomic data collected during experimental evolution in large, genetically diverse populations of *Drosophila melanogaster* to directly measure the manifestation of trade-offs in response to temporally fluctuating selection pressures on ecological timescales. Specifically, we quantify the genome-wide signal of antagonistic pleiotropy suggestive of trade-offs between reproduction and stress tolerance. We further identify a putative role of two cosmopolitan inversions in these trade-offs, and show that loci responding to selection during lab-based, reproduction selection exhibit signals of fluctuating selection in an outdoor mesocosm exposed to natural environmental conditions. Our results demonstrate the utility of time-series genomic data in revealing the presence and genomic architecture underlying fitness trade-offs, and add

credence to models positing a role of generic life history trade-offs in the maintenance of variation in natural populations.

Introduction

A fundamental tenet of evolutionary theory is that trait adaptation is restricted by trade-offs: the cost to individual fitness when an advantageous change in one trait occurs at the detriment to another (Roff and Fairbairn, 2007; Stearns, 1989). Trade-offs can be observed across closely related species, such as those between beak and body size among Darwin's finches (Grant et al., 1985; Shoval et al., 2012). They can also arise as a consequence of microevolutionary processes among populations of the same species; for instance, the trade-offs to survival associated with distinct reproductive strategies among populations of salmon (Christie et al., 2018). Trade-offs oftentimes emerge, and are most readily studied, in the context of life-history traits, and form the basis of the theory of life history evolution (Stearns, 1989). Ultimately, a key theoretical implication of trade-offs is that they maintain variation in fitness by constraining the simultaneous optimization of traits important for different environmental conditions (Charlesworth, 1994; Curtsinger et al., 1994; Rose, 1982; Stearns, 1989).

At the molecular level, trade-offs likely reflect antagonistic pleiotropy, a phenomenon in which an allele that enhances one fitness-related trait may simultaneously impede another. Crucially however, since only a subset of traits may positively impact fitness in a given environment, selection on the allele is not net-neutral, but instead flips direction when the environment changes (Curtsinger et al., 1994; Mitchell-Olds et al., 2007; Rose, 1982). Thus, a widely used method for inferring the presence of antagonistic pleiotropy and trade-offs is to compute genetic (co) variances using phenotypic data (A A Hoffmann and Parsons, 1989; Schmidt et al., 2005; Schou et al., 2022). Still, a more explicit way to quantify trade-offs, and also link them to the maintenance of variation, would be to directly measure population allele frequencies over time while selective pressures fluctuate. Indeed, several recent studies observed genome-wide fluctuations in allele frequencies through time, and across several distinct systems, suggesting underlying trade-offs (Bergland et al., 2014; Bitter et al., 2024; Machado et al., 2021; Rudman et al., 2022; Tataru et al., 2024; Troth et al., 2018).

A fundamental life-history trade-off is the balance between directing energy either towards survival or reproduction whereby periods of stressful environmental conditions favor somatic maintenance at the cost of reproductive investment (Flatt et al., 2013). This tradeoff is clearly apparent among populations of *Drosophila melanogaster* inhabiting temperate environments, a well-studied system in which increased food accessibility and warmer climates during summer spur exponential population growth, followed in winter by harsher conditions and population collapse (Band and Ives, 1961; Gleason et al., 2019; Ives, 1945). These cyclical

71 boom-bust population dynamics occur over approximately 10 generations and coincide with
72 the evolution of several classic life history traits: traits conferring increased reproduction (e.g.,
73 fecundity, faster developmental rates) are favored during spring and summer as populations
74 expand, followed by an increase in stress tolerance traits (e.g., desiccation and starvation
75 resistance) throughout the harsh winter and subsequent population collapse (Behrman et al.,
76 2015; Behrman and Schmidt, 2022; Boulétreau-Merle et al., 1987). It is likely that trade-offs
77 underpin these contrasting patterns of adaptation, as negative genetic correlations have been
78 quantified between seasonally evolving reproduction and stress tolerance traits (A A Hoffmann
79 and Parsons, 1989; Ary A. Hoffmann and Parsons, 1989; Service, 1987; Zera and Harshman,
80 2001).
81 Recent genome-wide sequencing of wild populations, and outbred populations evolved
82 in semi-natural mesocosms, has revealed evidence that hundreds of independent loci exhibit
83 signatures of selection concurrent to these patterns of rapid phenotypic evolution, many of
84 which switch in sign in concert with the fluctuating environment and evolving traits (Bergland
85 et al., 2014; Bitter et al., 2024; Machado et al., 2021; Rudman et al., 2022). Strikingly, despite
86 differences in the particular environmental conditions in which patterns of evolutionary change
87 were assayed (e.g., different observation years and geographic locations), there is high
88 repeatability in the genomic regions subject to fluctuating selection across space and time
89 (Bergland et al., 2014; Bitter et al., 2024; Machado et al., 2021). This suggests that the shared
90 genomic signals of temporally varying selection could be underpinned by a generic response
91 elicited by fundamental, life-history trade-offs. However, in the context of the natural
92 environments in which these studies were conducted, it is exceptionally challenging to
93 decompose which specific environmental pressures and fitness-relevant traits may interact to
94 produce trade-offs and maintain variation in the system. For example, it is unknown whether
95 the magnitude of phenotypic and genomic evolutionary change can be solely attributed to
96 shifting ecological pressures, such as population expansion and collapse; or, whether the
97 interaction of intraspecific ecological processes and changing abiotic conditions (e.g.,
98 temperature and precipitation) is necessary to solicit such dramatic adaptive responses and
99 reversions in allele frequency trends. Decoupling these selective forces, and directly linking
100 them to specific traits and patterns of allele frequency change, would be more robustly
101 addressed in the context of simplified and controlled experimental settings.
102 Here, we used two lab-based experimental evolution studies to more explicitly link key
103 components of life history evolution to patterns of fluctuating selection and maintenance of
104 variation in *D. melanogaster*. In the first of these studies, we assayed the impact of ecological
105 shifts, independent from any environmental selection. To do so, we monitored patterns of
106 genomic variation in genetically diverse, replicate populations housed in a controlled, indoor

environment throughout eleven discrete (non-overlapping) generations of population expansion, and a single bout of population truncation (Fig. 1; Fig S1). Our replicate populations were derived from a reconstituted, outbred population initiated from 145 inbred (DGRP) lines (Methods; Supplementary Data File 1), and evolution proceeded in four replicate cages (2 m^3). Food availability in the replicate cages was commensurate with increasing population sizes during the expansion phase, generating a selective regime that eliminated the impact of intraspecific competition (e.g. for food or egg laying space) and favored the reproduction-associated traits expected when resources are abundant, such as fecundity and developmental rate (Behrman et al., 2015). Contrarily, population truncation was induced by removing all food and water from our replicate cages and sampling the surviving individuals as the replicates collapsed. This mirrors dynamics of a population that has exceeded carrying capacity and, in effect, selects for the ability to withstand depleted resources via stress-tolerance mechanisms (Del Monte-Luna et al., 2004), which in our experiment is most likely to be desiccation resistance (Da Lage et al., 1989). We hypothesized that these contrasting selective regimes (hereafter, 'reproduction' and 'stress-tolerance' selection) would reveal trade-offs between life-history variation, whereby antagonistically pleiotropic alleles favored during sustained population expansion would become selected against during truncation.

The second experiment leveraged an independent inbred panel to construct a genetically diverse, outbred population, which was split into sets of indoor cage (N = 10) and outdoor mesocosm (N = 12) replicates. Through this, we used the same mapping population (thereby eliminating any confounding impacts of differences in linkage disequilibrium) to directly test whether loci identified under isolated selection for fast reproduction in the lab display predictable patterns of selection and antagonistic pleiotropy during adaptation in complex natural environments. In concert, our results provide evidence for: (1) strong, parallel selection induced under sustained population expansion (2) genome-wide tradeoffs associated with contrasting selective regimes of population expansion and truncation, (3) the role of cosmopolitan inversions underpinning fitness trade-offs during population expansion and collapse and (4) relevance of the alleles responding to selection for increased fecundity in a lab-based experiment to patterns of selection during adaptation to natural environmental fluctuations.

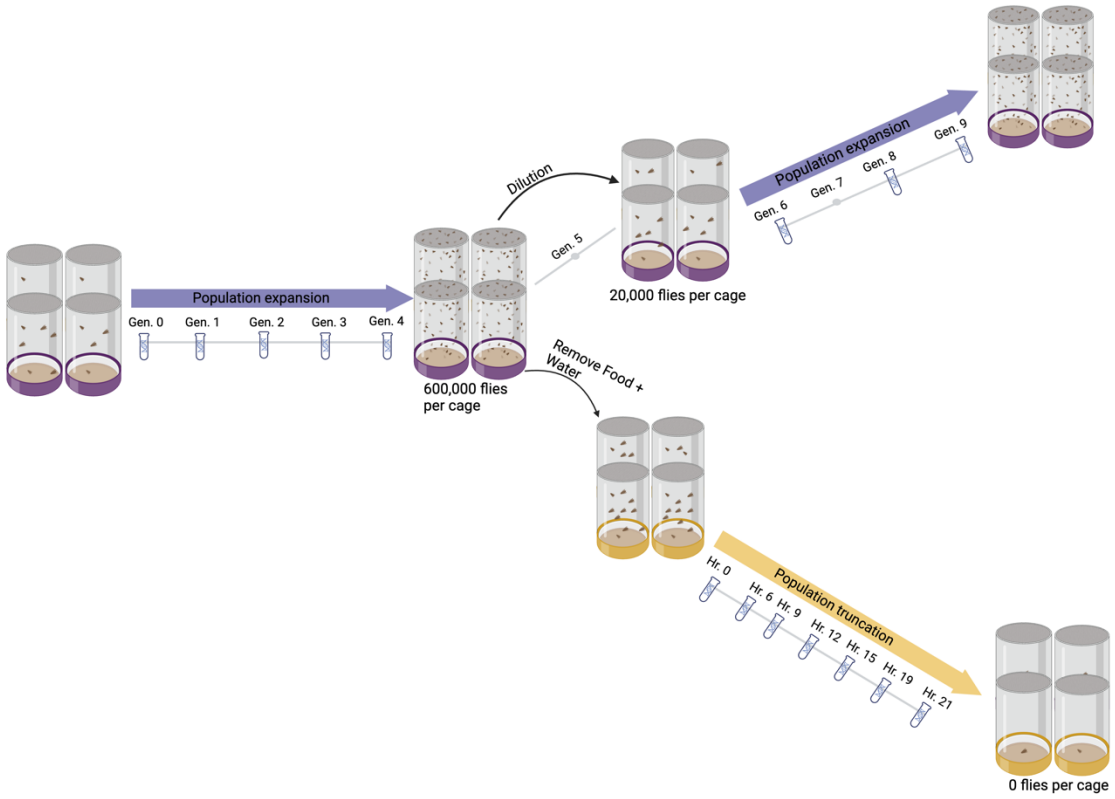

Figure 1. Schematic of lab-based, population expansion-truncation selection experiment | Four replicate, 2 m^3 cages were seeded with a genetically diverse, outbred population generated via four generations of recombination (N = 145 inbred lines). Evolution proceeded in discrete generations, whereby the amount of food was doubled every generation until replicate populations reached a census size of approximately 600,000 flies per cage (generation four). At this point, eggs from the generation 5 cohort were collected and all food and water was removed from the replicate cages. The adult cohort of the generation 4 flies was then sampled at seven time points (hours 0-21) as the absence of resources collapsed the populations. The generation 5 eggs were used to re-seed the replicate cages, which underwent continued population expansion for four additional generations. DNA in vials denotes generations of expansion, and hours of truncation, during which pooled samples were collected for pooled allele frequency calculation. Schematic generated with bioRender (https://www.biorender.com/).

Results

Selection during population expansion elicits genome-wide signals of strong, parallel selection

We observed parallel shifts in allele frequencies across the four replicate populations throughout the progression of population expansion, indicating adaptive responses to the shared selective pressures imposed in our experimental system. We quantified these systematic

159 allelic shifts using several approaches. We first computed genome-wide divergence as average
160 F_{ST} across all segregating sites pairwise among all expansion samples and used these data to
161 carry out several tests. F_{ST} divergence from the generation 0 populations increased steadily
162 within each cage through time, readily exceeding differentiation between biological replicates (F
163 = 172.2; p-value < 0.01; Fig. 2A & Fig. S2). We then used pairwise F_{ST} values as a distance metric
164 to create multi-dimensional scaling (MDS) plots, in which divergence between samples is
165 represented as distance among the points in a 2-D plane. Coloring samples based on the
166 replicate cage identity indicated that genome-wide allele frequencies in one replicate were
167 perturbed, shifting its points from the remaining three replicates throughout expansion (Fig.
168 2B). We hypothesize this was likely a result of potential bottlenecks during replicate cage
169 founding. However, despite this offset, samples from all cages appeared to shift across the 2-D
170 plane in the same direction through time, suggesting that the replicate populations experienced
171 parallel shifts in genome-wide allele frequencies (Fig 2C and Fig S3; a trend that was also
172 detected using principal component analysis; Fig. S4).
173 To more rigorously quantify the systematic movement of samples through time
174 observed in the two-dimensional MDS space, we translated coordinates for each cage such that
175 the centroid of all generation 0 samples was centered at the origin. We then used these
176 translated points to fit a simple linear regression model to samples from expansion generations
177 0-4 (Methods; Fig. S5). The resulting axis represents the primary axis of variation in the 2D
178 plane during early expansion for each replicate. We hypothesized that if sustained, directional
179 selection imposed by population expansion was a primary driver of patterns of genomic
180 variation, samples from the remaining expansion generations (generations 6-9) would continue
181 to proceed along the established axis of variation in the same direction. Indeed, projection of
182 late expansion samples onto this axis of variation indicated a significant correlation of sample
183 collection generation and distance along the axis (Fig 2D.; significance of correlation determined
184 via permutations). When segregating this analysis by chromosomal arm, however, this
185 parallelism was only evident on chromosomal arms 2L, 3L, and 3R ; while correlations derived
186 from SNPs on 2R and X were indistinguishable from permuted values (Fig. 2D). We re-sampled
187 SNPs across the genome iteratively to match the number present on each chromosomal arm to
188 confirm that the variation in parallelism was not a technical artifact. In each case, our sub-
189 sampling yielded correlations that matched the genome-wide trend, indicating that differences
190 observed among chromosomal arms (Fig. 2D) reflect systematic differences in the behavior of
191 loci across the genome (Fig. S6, Table S2).
192 To determine the distribution of SNPs (N = 1.7 M SNPs) contributing to the parallel
193 patterns of divergence across cages, a generalized linear model was fit to allele frequencies from
194 all expansion samples (generation 0-9). This model assessed the significance of the linear

195 relationship between allele frequency and generation of sampling across all cages, using a
196 quasibinomial error model to reduce false positive associations (Machado et al., 2021; Rudman
197 et al., 2022; Wiberg et al., 2017). While an association between allele frequency and sampling
198 timepoint within a single cage may represent either drift or selection, a significant parallel
199 association across all four replicate cages indicates allele frequency trajectories that are both
200 predictable over time and parallel across populations. In this case, selection (or linked selection)
201 is the more parsimonious explanation. A total of 389,588 SNPs (22.9 % of all sites), across all
202 chromosomal arms, showed significant parallelism after multiple testing correction (Benjamini-
203 Hochberg false discovery rate <0.01 and allele frequency change > 2%). These SNPs showed
204 systematic, directional selection across replicates throughout expansion (Fig. 2E; Fig. S7).
205 Furthermore, the genomic distribution of these SNPs spanned all five chromosomal arms and
206 were located both within and outside the breakpoints of five major cosmopolitan inversions
207 that segregated at appreciable frequency (>4%) in our inbred reference panel (Fig. 2F).
208 We validated the parallelism inferred by GLM by implementing a leave-one-out cross
209 validation. Specifically, we iteratively identified sets of parallel SNPs across expansion samples
210 using a GLM fit to allele frequency data from three of the four replicate cages. We then
211 quantified the frequency shifts of the rising allele at significant SNPs (FDR < 0.01, allele
212 frequency shift > 2 %) in the left-out cage. In each iteration of this analysis, the left-out cage
213 exhibited a magnitude of allele frequency change that exceeded the background allele
214 frequency change (quantified using matched control SNPs; see Methods), and in a direction of
215 change parallel to that observed in the other three cages (Fig 2G). The genome-wide median
216 shifts of target SNPs across replicates ranged between 5 and 7.5%, indicating that these parallel
217 patterns of adaptation were underpinned by strong selection, on the order of 10-20% per
218 generation. While the per-chromosome Fst and MDS analyses described above, which focus on
219 signal averaged across all segregating sites, suggest that non-parallel idiosyncratic movement
220 may be the dominant force on certain chromosomes, our GLM analysis parallel SNPs can still
221 be discovered on every chromosomal arm.

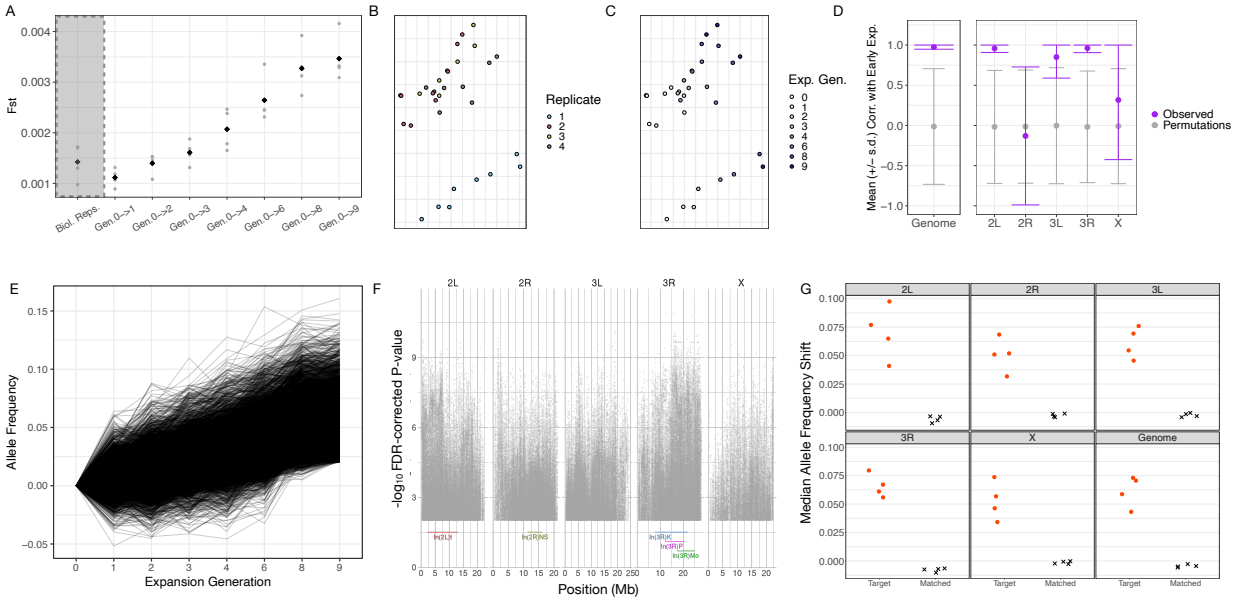

Figure 2. Adaptation under sustained population expansion elicits strong, genome-wide parallel responses | (A) Mean, genome-wide F_{ST} between biological replicates ('Biological Replicates'; same replicate/collection time point, different pooled sample/extraction of flies) and evolved replicate samples and their respective generation 0 expansion sample ('Gen. 0->n'). Grey points indicate individual replicate samples, and black diamonds the averaged value across replicates. F_{ST} differentiation from generation 0 samples increased monotonically as function of collection time ($F = 172.2$; p-value < 0.01). (B-C) MDS of F_{ST} values computed pairwise across all expansion samples, colored according to (B) replicate cage or (C) collection generation. (D) Average Pearson Correlation across replicates (+/- standard deviation) between sample expansion generation and distance along a one-dimensional axis constructed using F_{ST} MDS coordinates for early expansion (generation 0-4) samples (Fig. 2C). Purple points and error bars correspond to observed values (mean +/- standard deviation across cages), while grey points and error bars correspond to values derived from $N = 100$ permutations. (E) Trajectories of rising alleles at SNPs identified via GLM (FDR < 0.01 and effect size $> 2\%$) across all nine generations of expansion. (D) Genomic distribution of SNPs depicted in (E). The coordinates of the major cosmopolitan inversions segregating in our founding reference panel at greater than 4% frequency in our founding strains are depicted above the x-axis. (G) Leave-one-out cross-validation to infer replicate-specific parallelism of adaptation to sustained population expansion. Portrayed is the median shift of the rising allele for sets of target SNPs (points) identified via GLM (FDR < 0.01 and effect size $> 2\%$) in 3 of 4 cages, relative to medians derived from a matched control SNP set (X's), in the left-out replicate. Target SNP medians are colored red if the distribution of phased allele frequency shifts was significantly greater than that of matched control sites (two-tailed t-test, FDR < 0.05).

Genomic evidence of trade-offs induced by fluctuating selection across expansion and truncation

The parallel frequency shifts observed throughout expansion may be the product of three, not mutually exclusive, evolutionary dynamics: (1) directional selection in response to sustained fecundity selection, (2) adaptation to the lab environment, and/or (3) the purging of recessive deleterious alleles (i.e., negative selection) in outbred population. To disentangle these

248 various dynamics and, in turn, identify the presence of fitness-tradeoffs at putatively selected
249 alleles, we leveraged our samples collected throughout truncation selection. Alleles identified
250 during expansion that were a product of consistent lab selection and/or negative selection
251 against unconditionally deleterious recessives should continue to show systematic, directional
252 change throughout truncation (as their effect is not conditional on the specific treatment).
253 However, alleles with treatment-specific behavior during expansion and truncation (i.e.,
254 moving in the opposite direction) represent those that likely underpin trade-offs between
255 fecundity and stress tolerance selection.
256 We tested for evidence of context-specific behavior and trade-offs of genome-wide SNPs
257 by re-conducting our MDS analysis of pairwise divergence values, this time including all
258 samples collected throughout expansion and truncation. If the dominant direction of allele
259 frequency change was sustained across both expansion and truncation (indicating sustained lab
260 selection or purging of deleterious mutations), truncation samples would be ordered from early
261 to late in a parallel manner as the expansion samples (Fig 2B). Instead, we observed that
262 samples taken during truncation (initiated at expansion generation 5) shifted back towards
263 earlier expansion samples, potentially suggesting a genome-wide reversion of allele frequencies
264 (Fig. 3A; Fig. S8). We quantified these trends as above, translating the MDS coordinates of each
265 truncation sample such that the centroid of all hour 0 samples was centered at the origin and
266 then projecting them onto a the single axis linear regression model derived from early
267 expansion points (Fig. 2D; Fig. S5). As hypothesized, correlations between collection time and
268 distance along this axis were, genome-wide, significantly negative (Fig. 3B; Table S1).
269 Segregating this analysis by chromosomal arm yielded more nuanced dynamics whereby 3L,
270 3R, and X yielded evidence of anti-parallel/reversions in allele frequencies, while 2L and 2R
271 exhibited correlations that were insignificant relative to our permuted distributions (Fig. 3B).
272 Again, as above, we validated that these differences among chromosomal arms were not simply
273 a reflection of variation in number of SNPs available for measurement and reflected systematic
274 differences in allele frequency dynamics across the genome (Fig. S9).
275 We garnered further evidence of trade-offs across fecundity and desiccation selection
276 using allele frequency trajectories. Specifically, we selected those SNPs with evidence of
277 systematic movement across replicates throughout expansion (GLM FDR < 0.01 and allele
278 frequency shift $> 2\%$) and measured the average frequency shifts of the rising allele across cages
279 throughout truncation (Figure 3D). If patterns of fluctuating selection and antagonistic
280 pleiotropy dominated the data, we expected trajectories to be enriched for SNPs moving in the
281 opposite (negative) direction during truncation. Indeed, across all expansion-identified SNPs,
282 the ratio was significantly skewed towards those with exhibiting fluctuating selection, as

283 opposed to sustained directional selection, across expansion and truncation selection (χ^2 =
284 1123.6; P-value < 0.001). These trajectories are depicted in Figure 3D, in which colored
285 trajectories indicate those expansion-identified SNPs with additional, independent evidence of
286 systematic movement across cages during truncation (GLM FDR < 0.05 and effect size > 1%):
287 purple for those SNPs with consistent directional selection across selection regimes, and orange
288 for those with anti-parallel movement across regimes. As expected, this subset of SNPs (*N* =
289 24,814) exhibited even greater evidence of fluctuating selection and were 3.5 times more likely
290 to fluctuate directions across treatments than exhibit sustained directional selection (19,158
291 relative to 5,656 SNPs, respectively). We assessed how consistent this dynamic was across the
292 genome by quantifying the ratio of parallel vs. fluctuating selection genome-wide, and
293 separately for each chromosomal arm. As expected based on the F_{ST} MDS analysis described
294 above, there was strong evidence of enrichment for fluctuating selection on chromosomal arms
295 3L, 3R, and X. However, this analysis revealed an enrichment of 2L SNPs with sustained
296 parallel selection across selection regimes, which was an undetected in our F_{ST} MDS analysis.
297 We explored this dynamic further, using the underlying allele frequency shift distributions to
298 compute empirical cumulative distribution functions, separately for alleles with sustained
299 directional selection and for those with evidence of fluctuating selection (See Supp. Mat.). This
300 verified an enrichment of alleles exhibiting fluctuating selection on arms 3L, 3R, and X, and
301 sustained directional selection on 2L (Fig S10). In conclusion, we find evidence for the existence
302 of pervasive, genome-wide trade-offs between fecundity and desiccation selection, as well as
303 some evidence of sustained directional selection due to either adaptation to the lab environment
304 or purging of the unconditionally deleterious alleles. It is important to note the patterns of
305 fluctuating selection quantified here cannot be a spurious artifact driven by regression to the
306 mean, as the data from which the trajectories were computed are entirely independent across
307 expansion and truncation because they share no common datapoints.
308
309
310
311
312
313
314
315
316
317
318
319
320

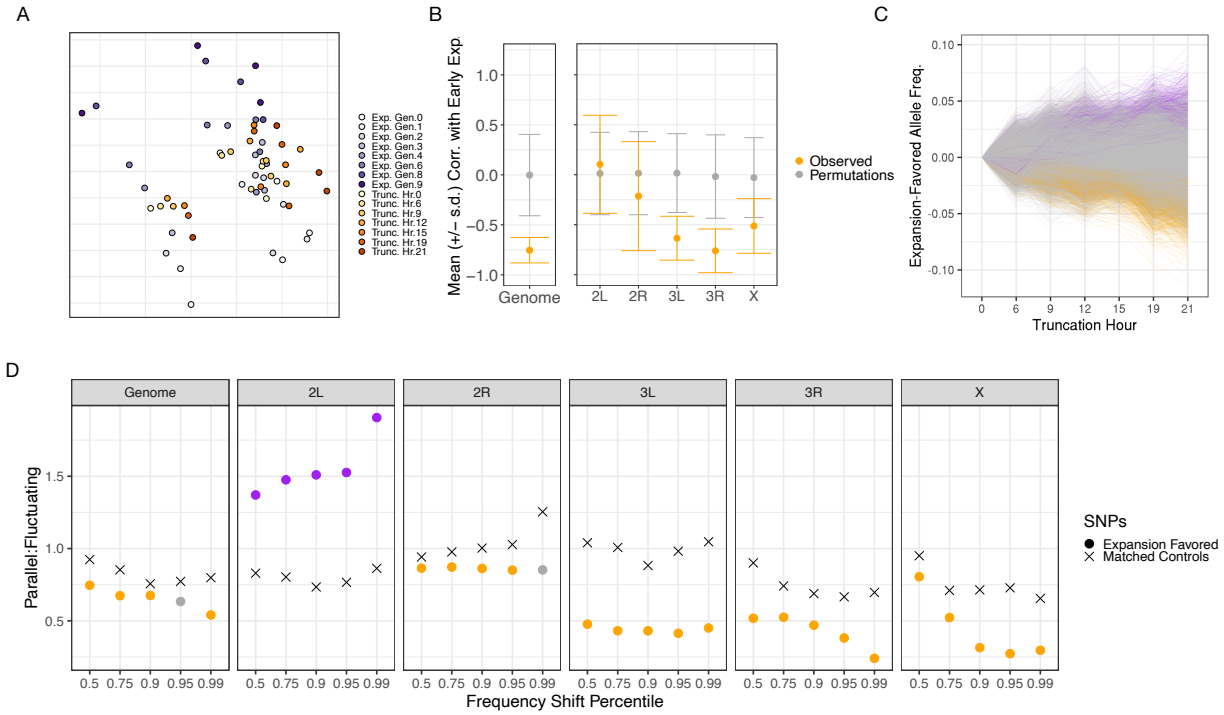

Figure 3. Genome-wide signal of fitness trade-offs between population expansion and truncation | (A) MDS of pairwise F_{ST} values across all samples collected throughout expansion (purple-hue points) and truncation (orange-hue points), shaded according to collection time point (darker hues indicate later expansion or truncation sampling generation/hour. (B) Average Pearson correlation across replicates (+/- standard deviation) between sample expansion generation and distance along a one-dimensional axis constructed using F_{ST} MDS coordinates for early expansion (generation 0-4) samples (Fig. 3A). Orange points and error bars correspond to observed values (mean +/- standard deviation across cages), while grey points and error bars correspond to values derived from N = 100 permutations. (C) Trajectories of SNPs identified via GLM regression across replicates throughout expansion, measured during truncation. Trajectories are colored for SNPs that exhibited evidence of systematic allele frequency changes across replicates during truncation (GLM FDR < 0.05 and allele frequency change > 1%) and displayed sustained directional (purple) or fluctuating selection (orange). (D) Ratio of parallel to fluctuating dynamics for expansion-favored alleles during truncation, segregated by chromosomal arm and percentile of truncation allele frequency shift. Points are further colored if the ratio of parallel to fluctuating behavior differed significantly from that expected based on a matched control set (χ^2 test P-value < 0.05).

The role of inversions in reproduction/stress-tolerance trade-offs

Theoretical, and emerging empirical, research suggests a dominant role of chromosomal inversions in adaptation in natural populations (Berdan et al., 2023). Accordingly, we quantified whether five major cosmopolitan inversions in *D. melanogaster* (*In(2L)t*, *In(2R)NS*, *In(3R)K*, *In(3R)P*, *In(3R)Mo*), which all occurred at starting frequency > 4% in our inbred reference panel, exhibited dynamics consistent with adaptation and, if so, trade-offs between population expansion and truncation (Supplementary Data File 3). Generalized linear regression of inversion frequencies yielded evidence that all inversions shifted systematically across replicates during expansion, with magnitude of frequency shifts ranging between 1 and 7% (Fig. 4A-E; Table S2). *In(3R)K* and *In(3R)P* were the only two inversions that exhibited evidence of trade-offs across selection regimes, whereby each inversion was systematically favored during expansion and then became selected against during truncation (Fig. 4A-B).

Given the appreciable effect of inversions on patterns of adaptation throughout the experiment, we next explored the extent to which our inference of trade-offs was solely a function of variation within, or in tight linkage of, these structural variants. Specifically, we reconducted F_{ST}-based MDS analysis on a subset of SNPs, excluding all those within, or 100 kb away from, inversion breakpoints. Through this, we observed that the signal of reversions in allele frequencies were maintained on 3L and X, but eliminated on 3R. Still, the genome-wide signal of this analysis continued to indicate parallel movement across early and late-expansion samples, and that a signal of fluctuating selection dominates patterns of genomic variation between expansion and truncation (Fig. S11). We validated that this trend was not simply a function of the reduced set of SNPs available for analysis, relative to the genome-wide panel (Fig. S12).

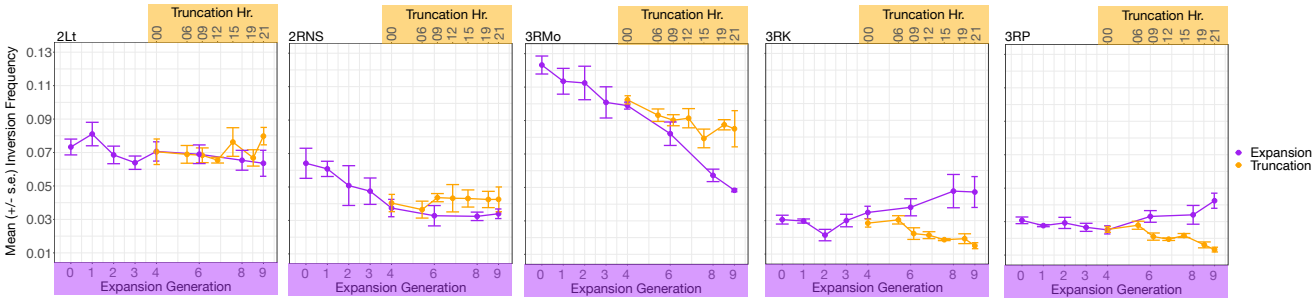

Figure 4. Role of inversions in reproduction and stress-tolerance trade-offs | Mean inversion frequency changes (+/- s.e.) across expansion generations (purple trajectories) and truncation hours (orange trajectories).

373 *The emergence of tradeoffs in response to natural environmental fluctuations*

374 We quantified whether alleles identified via selection under sustained population
375 expansion in a laboratory setting can predict patterns of adaption and trade-offs in an outdoor
376 environment, where populations adapt both to changes in population density as well as a suite
377 of additional abiotic variables. Specifically, we leveraged data from an independent study year
378 when we monitored patterns of genomic variation in a genetically diverse population that was
379 split into a series of large, replicate cages maintained in both a controlled, indoor laboratory (N
380 = 10 replicate populations), as well as outdoor mesocosms exposed to natural environmental
381 fluctuations (N = 12 replicate populations; data previously reported in Bitter et al. 2024) (Fig.
382 S13). As with our indoor expansion/truncation experiment described above, the population
383 used in this experiment was derived via outbreeding an inbred reference panel, which in this
384 case was originally collected from Linvilla Orchards, Media, PA (Supplementary Data File 2).
385 The replicates in both environments evolved with overlapping generations, under constant food
386 conditions, for a period of four months (see Methods). This induced rapid population expansion
387 in each environment until a peak/stabilization of density was observed, suggesting the
388 initiation of density control (Fig. S11; Table S7).

389 We first quantified the extent to which evolution in the outdoor environment is driven
390 by the selective pressures solely associated with increasing population density (e.g., selection
391 for increased fecundity, faster developmental rate). Specifically, we identified alleles
392 systematically favored throughout concurrent sampling of the indoor and outdoor cages using
393 a GLM (see Methods), and found far greater overlap than expected based on matched control
394 SNPs (Fig. 5A). Next, we asked whether the dominant direction of selection was parallel across
395 environments by quantifying frequency shifts in the outdoor replicates at the rising allele for
396 each SNP identified within the indoor environment. We observed that the magnitude of allele
397 frequency shifts was significantly greater than background allele frequency movement, and that
398 the dominant direction of selection was conserved between environments (indicated via
399 positive median shifts depicted in Fig. 5B; Table S6).

400 Finally, we tested whether the pervasive trade-offs we inferred from the previous
401 experiment and results described above (Fig. 1-4) manifested in the outdoor mesocosms.
402 Specifically, we leveraged an additional month of sampling in the outdoor mesocosms, during
403 which time a population decline and ultimate collapse was observed as winter and the
404 deterioration of abiotic conditions progressed (Bitter et al., 2024). We hypothesized that, should
405 those alleles identified in the indoor environment underpin antagonistic pleiotropy and trade-
406 offs for fitness-relevant variation, allele frequencies should reverse in direction as the outdoor
407 mesocosms collapsed. Indeed, we found a subtle, but significant genome-wide reversion in

allele frequencies in the outdoor cages throughout this period, which was ultimately driven by patterns of variation on 2L and 3R (Fig. 5C; Table S6).

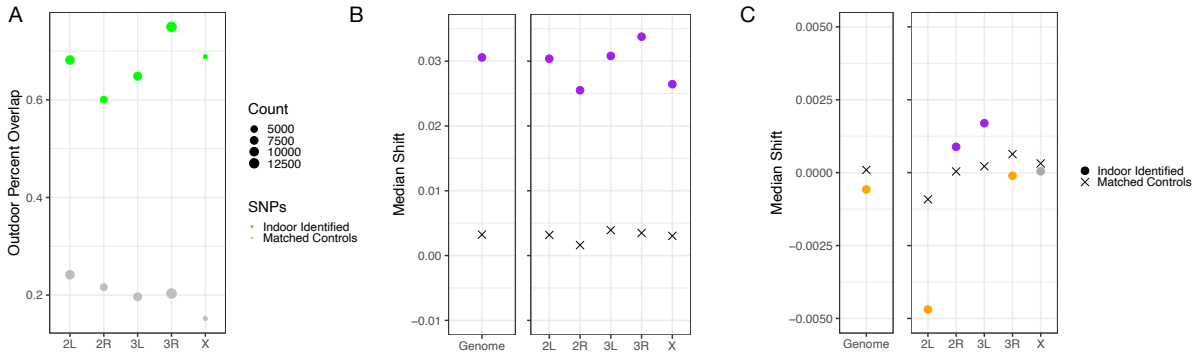

Figure 5. Selection on reproduction under controlled, lab-based conditions predicts patterns of adaptation and trade-offs in outdoor mesocosms | (A) Observed vs. expected overlap in SNPs with systematic allele frequency movement (GLM FDR < 0.01; allele frequency change > 2%) in a paired indoor and outdoor experimental evolution study. (B-C) Median shift of alleles identified during expansion in an indoor environment, quantified during population expansion (B) and collapse (C) in an outdoor mesocosm. Colored circles correspond to indoor-identified SNPs with allele frequency shift distributions that were either significantly greater (orange) or less (purple) than that observed for matched control SNPs (X's) (two-tailed t-test FDR < 0.05).

Discussion

We quantified genome-wide evidence of fitness trade-offs in response to selection on two key life-history traits in the context of ecologically realistic population boom and bust population dynamics. Our results hold relevance for the maintenance of fitness-relevant variation, the genomic basis of fitness-tradeoffs, and the interplay of ecological and evolutionary processes in natural populations.

We manipulated reproduction selection via nine generations of sustained population expansion in the absence of density regulation mechanisms. This process induced parallel, genome-wide shifts in allele frequencies across four, independent replicate populations. The strong selection coefficients quantified throughout this period (~10% per generation) are comparable to those quantified during sampling between summer and fall in wild populations and outdoor mesocosms (Bergland et al., 2014; Bitter et al., 2024; Machado et al., 2021; Rudman et al., 2022). Thus, while it has been previously speculated that such patterns of evolution of *D. melanogaster* across seasons may be dominated by adaptation to shifting temperatures (e.g., Boulétreau-Merle, Fouillet, and Terrier 1987), our lab-based manipulation here provides direct evidence that the sole impact of shifting population densities can drive rapid adaptation over the course of several generations. In effect, this finding bolsters the notion that the interaction of

436 ecological and evolutionary forces may be a fundamental force acting within natural
437 populations (Carroll et al., 2007; Hendry, 2016).
438 By imposing a bout of truncation selection midway through population expansion,
439 during which time individual survival and associated patterns of allele frequency change
440 revealed differences in relative stress tolerance (e.g., desiccation resistance) among genotypes,
441 we aimed to explore evidence of fitness-tradeoffs in the system. We quantified a pervasive,
442 genome-wide signal of fluctuating selection, whereby patterns of allele frequency movement
443 reversed direction across selection regimes. These patterns are indicative of antagonistic
444 pleiotropy, whereby selected alleles conveying advantageous trait values for the phenotypes
445 favored during reproduction selection convey disadvantageous trait values for the suite of
446 phenotypes favored during truncation (Connallon and Chenoweth, 2019; Curtsinger et al.,
447 1994). While this dynamic was *a priori* expected based on the negative genetic correlations
448 between traits likely under selection in our experiment (A A Hoffmann and Parsons, 1989; Ary
449 A. Hoffmann and Parsons, 1989; Service, 1987; Zera and Harshman, 2001), few data exist
450 directly observing the manifestation of such trade-offs, particularly over the ecologically-
451 relevant timescales assayed in our experiment. The key implication of this antagonistically
452 pleiotropic behavior is that this process may, in effect, maintain variation in the population
453 (Curtsinger et al., 1994; Rose, 1982). Specifically, mutations with unconditionally advantageous
454 effects will ultimately be driven to fixation, while those with context-specific behavior can in
455 principle be maintained for longer periods of time in the presence of fluctuating selective
456 pressures (Turelli and Barton, 2004; Wittmann et al., 2017). The key challenge for future work
457 will be to discern whether these dynamics indeed balance alleles over long time-periods, which
458 will ultimately be aided by refining the causal loci driving the patterns observed here and
459 observation across multiple bouts of fluctuating selection.
460 The genomic architecture of trade-offs was not dominated by a single, large-effect locus,
461 nor were antagonistically pleiotropic alleles distributed evenly across chromosomal arms.
462 Rather, we quantified a dominant signal of fluctuating selection across reproduction and stress-
463 tolerance selection on chromosomal arms 3L, 3R, and X, and extensively showed that this signal
464 was not spurious due to variation in the number of SNPs available for analysis across arms. We
465 further showed that the trade-offs quantified on 3R were likely underpinned by inversions
466 segregating in our experimental population. Inversions are a common form of structural
467 variation both across species and within populations and have long been recognized as
468 important for adaptive evolution. For example, suppressed recombination within the
469 breakpoints of relatively young inversions can give rise to the accumulation of putatively
470 adaptive alleles (Kirkpatrick, 2010; Kirkpatrick and Barton, 2006; Sturtevant, 1921; Sturtevant
471 and Beadle, 1936). Indeed, in natural populations of *D. melanogaster*, inversions are implicated in

472 adaptation to spatially and temporally varying selection pressures, which may, in part, be
473 underpinned by the selective pressures manipulated in our lab-based study (Kapun et al., 2023,
474 2016; Machado et al., 2021; Nunez et al., 2024). We add to this growing body of research, here
475 reporting evidence for a role of each of five major chromosomal inversions during reproduction
476 selection, with two of these inversions, *In(3R)P*, and *In(3R)K*, showing a behavior consistent
477 with trade-offs between reproduction and stress-tolerance selection. In congruence with this
478 result, previous experimental work has demonstrated that inverted karyotypes of *In(3R)P* are
479 shorter-lived and less stress resistant than non-inverted karyotypes, as would be predicted
480 based on the frequency trajectories of this inversion in our experiment (Durmaz et al., 2018).
481 Still, resolving the functional relevance of each of these major inversions is nascent and
482 provides a fruitful avenue of future research.

483 It is noteworthy that the trade-offs quantified here manifested during a single bout of
484 truncation selection, which proceeded over the course of just 24 hours. This illustrates how
485 finely adaptation via standing variation can track shifting environmental conditions, and that
486 selection can be detected on temporal scales shorter than a single generation. Indeed, mounting
487 research has shown how both anomalous (e.g., heat wave, hurricane, or poaching) and non-
488 anomalous (e.g., weekly to seasonal shifts in abiotic and biotic conditions) environmental
489 perturbations can elicit patterns of adaptation on similar timescales in natural populations
490 (Bergland et al., 2014; Bitter et al., 2024; Campbell-Staton et al., 2021, 2017; Donihue et al., 2018;
491 Machado et al., 2021; Nunez et al., 2024; Rodríguez-Trelles et al., 2013; Rudman et al., 2022).
492 This growing body of research increasingly suggests that the selection coefficients
493 underpinning the standing, functional variation in natural populations may be substantially
494 larger than previously recognized, and ultimately augment adaptation to the accelerated shifts
495 in mean environments associated with global climate change.

496 Our paired indoor cage and outdoor mesocosm experiment demonstrated how selection
497 induced by population expansion under controlled, lab-based conditions can identify alleles
498 that are relevant to adaptation and trade-offs in response to natural environmental fluctuations
499 (Fig. 5). Such repeatability in the targets of selection suggests a set of shared selective pressures
500 acted across environments, which in this case are most likely those associated with changes in
501 population density (as abiotic conditions in the indoor environment were controlled). Thus, the
502 repeated signals of fluctuating selection quantified in *D. melanogaster*, both across populations
503 and through time (Bergland et al., 2014; Bitter et al., 2024; Machado et al., 2021; Rudman et al.,
504 2022), may be underpinned by fundamental life-history trade-offs that emerge as a result of
505 shifts in the selective environment induced by population boom-bust demographic dynamics.
506 These boom-bust demographic dynamics are a generic feature of populations across taxa, and
507 this phenomenon may thus be more widespread than previously recognized and provide a key

508 instance of the interplay of ecological and evolutionary forces in natural populations (Boor et
509 al., 2018; Carroll et al., 2007; Hendry, 2016; Kendall et al., 1999). Furthermore, given the
510 dramatic differences in indoor and outdoor environments, the shared allele frequency patterns
511 observed here suggest that core alleles may underpin adaptation during generic boom and bust
512 cycles, regardless of specific abiotic condition. Such a 'coarse-graining' of the architecture of the
513 adaptive response would position fluctuating selection as a key force in maintaining variation
514 in natural populations. While we note the possibility that a unique set of loci become fitness-
515 relevant under specific abiotic contexts, our goal here was to simply query whether a common
516 set of loci underpinned trade-offs and responded generically to fluctuating selection across
517 abiotic contexts, for which we found substantial evidence.
518 Finally, we observed differences in the architecture of trade-offs between our indoor
519 population expansion/trucnation selection experiment and the paired indoor-outdoor
520 mesocosm study. For example, chromosomal arm 2L displayed evidence of sustained selection
521 across reproduction and stress tolerance selection in the first experiment, but exhibited strong
522 evidence of antagonistic pleiotropy between population expansion and collapse during our
523 outdoor mesocosm experiment. Furthermore, we did not detect any shared enrichment of SNPs
524 with evidence of linked selection across these experiments. While there were distinct
525 methodological and environmental differences that may have played a role in this discordance,
526 a more salient possibility is the use of a different set of inbred lines to generate the outbred
527 mapping population for each experiment. As our analyses ultimately identify sets of SNPs in
528 tight linkage to an underlying causal locus, differences in patterns of linkage across mapping
529 populations could, in effect, lead to dramatic differences in the relative effect size of marker
530 alleles across studies. This process is analogous to the oftentimes poor portability of association
531 studies across human populations (de Bakker et al., 2006; Martinez et al., 2024), and is an
532 important consideration for future research using experimental evolution approaches to
533 characterize the architecture of complex trait adaptation.
534 In conclusion, the data presented here demonstrate how well-resolved time-series
535 genomic data can reveal the presence of, and genomic architecture underlying, fitness trade-
536 offs. Such trade-offs can emerge in response to generic shifts in intraspecific ecological
537 conditions and may in turn serve as a key force maintaining variation in natural populations.
538
539 **Methods**
540 *Population construction and replicate cage seeding for expansion/truncation selection experiment*
541 We constructed a genetically diverse founder population via outbreeding 145 lines of the
542 Drosophila melanogaster Genetic Reference Panel (DGRP; Mackay et al. 2012). Ten mated
543 females per DGRP inbred line, each of the same age cohort and from density-controlled line

544 cultures, were pooled into a single 0.3m x 0.6m x 0.3m cage (P0 generation). Over the course of
545 4d, eggs were collected in 64 culture bottles (P1 generation) using cornmeal molasses medium
546 (16 bottles added per day, then capped, removed, and 16 new bottles added); the 64 bottles
547 were then randomly assigned to 1 of the 4 replicate cages; from this point forward, all replicates
548 were cultured independently. Once flies eclosed, they were again released into 4 replicate 0.3m
549 x 0.7m x 0.3m cages, and eggs were collected over 24h on two culture trays (0.5m x 0.3m x 0.1m;
550 1L of Drosophila cornmeal molasses medium per tray) per replicate. Once these flies eclosed
551 (the first true F1 generation), the flies were released into 4 replicate, medium sized cages (0.6m x
552 0.6m x 1.2m) and allowed to oviposit on 4 trays of culture medium over 24h (embryos were the
553 F2 generation). The F2 embryos from these trays were sealed and collected, and the adults
554 discarded. Once the F2 flies eclosed, they were then released into large, experimental cages (3
555 m^3) and given 8 trays of media for oviposition over 24h.
556 *Population expansion/truncation selection in large, indoor cages*
557 Culturing within the large, experimental cages proceeded via discrete generations,
558 throughout which the amount of food was doubled every generation (starting at 8 trays for the
559 F2). By doubling food every generation we generated sustained population expansion, thereby
560 continually selecting for the fecundity-associated traits that are advantageous in wild
561 populations when resources are abundant, most likely reproductive output and increased
562 developmental rate. Hereafter, we refer to collection timepoints in accordance with the number
563 of generations since release into large cages (the first 8 tray stage), which was two generations
564 from the actual founding of the experimental populations (i.e., the samples labeled "generation
565 0" are F2's, "generation 1" are F3's, and so forth). Once flies had laid eggs for a period of 24h,
566 the adults were removed from each cage and their volume measured to estimate census size.
567 The remaining embryos (i.e., subsequent generation of flies) were left to develop and eclose
568 within the same replicate cage. Across replicates, the population sizes rapidly expanded across
569 generations, a dynamic selecting for individuals exhibiting increased reproduction (e.g.,
570 fecundity and developmental rate) (Fig. 1).
571 We maintained food doubling until generation 4 at which point, due to logistical
572 constraints, it was not possible to continue the doubling of population size per cage beyond the
573 64 tray per cage generation. In order to continue the selection regime of population expansion
574 (and selection for early fecundity, fast developmental rate), we instituted a random dilution
575 followed by re-expansion. Specifically, the fifth generation was founded with embryos collected
576 over 24h on two food trays (containing eggs of approximately 20,000 flies), from the from the
577 fourth generation. These generation 5 flies were allowed to develop and eclose in the large
578 indoor cages, at which point 8 trays of medium were added to each replicate cage, and
579 oviposition was carried out for 24h and after which adults were discarded. Once the sixth

580 generation of flies eclosed, they were allowed to oviposit for 24h on 2 food trays. These
581 generation 7 embryos were then allowed to develop, eclose, and expanded out to 8 trays for the
582 eighth generation. The generation 8 flies were allowed to oviposit over 24h on 8 trays,
583 consistent with the previous generation (thus each generation of flies resulted from egg laying
584 over a period of 24h from the preceding generation). We collected a random sample of 100 male
585 and 100 female flies in generations 0, 1, 2, 3, 4, 6, 8, and 9, and pooled sexes separately for later
586 whole genome shotgun sequencing (see below). We took additional samples of each replicate at
587 generations 6 and 8 to use as biological replicates (i.e., same replicate/generation, different set
588 of 100 flies) to quantify noise in our allele frequency estimates (see below). Census estimates
589 (based on the total volume of dead flies) of adult flies within each cage were conducted on
590 generations 1-4. Calibration of census estimates was conducted by counting the number of flies
591 (desiccated and dried) in $1cm^3$ and then measuring the volume in a given sample.
592 Concurrent to the generation 4 dilution and re-expansion described above, we induced a
593 bout of truncation selection that segregated flies based on stress-tolerance, most likely
594 desiccation resistance as water availability is expected to drive mortality at a much faster rate
595 than starvation (Da Lage et al., 1989). Specifically, after collecting generation 5 embryos for
596 continued expansion, we retained the adult flies within their respective cages, removed all food
597 and water, and sampled the surviving adults at various timepoints by direct aspiration using
598 vacuums until all flies had died. The live samples were immediately sorted by sex and
599 timepoint and preserved in ethanol (as with expansion samples, 100 male and 100 female flies
600 were isolated at each collection time point for whole genome shotgun sequencing). We
601 continued this process until there were an insufficient number of flies (i.e., < 100 individuals)
602 for sampling, resulting in samples for DNA analysis collected at hours 0, 6, 9, 12, 15, 19, and 21.
603 Samples collected throughout this process were expected to reveal changes in the relative
604 frequency of genotypes of differing degrees of stress-tolerance, traits expected to trade-off with
605 the reproductive traits favored during the nine generations of expansion selection (A A
606 Hoffmann and Parsons, 1989; Ary A. Hoffmann and Parsons, 1989).
607 *Pooled genomic sequencing and allele frequency estimation of expansion/truncation selection experiment*
608 Genomic DNA from pools of 100 male and 100 female flies were extracted and
609 sequenced in two rounds. First, multiplexed libraries were created for 56 expansion samples
610 using Illumina Nextera DNA Prep with e-gel size selection and i7 indexing. Barcoded fragments
611 were mixed and loaded evenly into 4 lanes, then sequenced with 100 bp paired-end reads on an
612 Illumina HiSeq2000 sequencer, with target coverage of 10x per sample. After QC, resulting
613 per/sample coverage was quite variable, and 26 samples from this round with coverage <2x
614 were later re-sequenced with 150-bp dual-indexed reads on an Illumina HiSeq4000 sequencer.
615 Reads from the same sample were merged after all QC and mapping steps. A separate round of

616 sequencing was conducted for the remaining 96 samples, including remaining expansion and
617 truncation samples. These samples were sequenced with 150-bp paired-end dual-index reads on
618 a NextSeq550 high output machine, with a target coverage 7x per sample. All samples were
619 demultiplexed, adapter sequences were trimmed, and reads with any 3′ bases with quality score
620 < 20 or trim length <18 were discarded. Overlapping forward and reverse reads were
621 subsequently assembled and reads were mapped separately to the *D.mel* v5.39 reference
622 genome using bwa and default parameters (Li and Durbin, 2009). Aligned reads were
623 deduplicated using Picard tools (http://broadinstitute.github.io/picard/), and all reads were
624 re-aligned around indels using GATK v4 IndelRealigner (https://gatk.broadinstitute.org/).
625 We used the founder line genome sequencing data to compute haplotype-informed
626 allele frequency estimates at 2.7 M, previously identified, segregating sites using a local
627 inference method and pipeline developed and described by (Kessner et al., 2013; Tilk et al.,
628 2019). We conducted haplotype inference in window sizes that varied proportionally to the
629 length of un-recombined haplotype blocks expected as a function of the estimated number of
630 generations since the construction of the outbred population. We have previously provided
631 extensive validation that our haplotype-informed allele frequencies are replicable across
632 different sets of subsampled reads from the same sample, and produce an accuracy of allele
633 frequency estimates that is comparable to deep sequencing and standard methods for pooled,
634 allele frequency estimation (Bitter et al., 2024; Rudman et al., 2022; Tilk et al., 2019). We filtered
635 our allele frequencies to only include those sites with an average minor allele > 0.02 across all
636 samples, resulting in 1.7M SNPs for analysis. Finally, we averaged technical replicate allele
637 frequencies (i.e. the male and female pool) for each replicate and collection time point, resulting
638 in 4 cages per time point, across 8 expansion generations and 7 truncation time points (60 total
639 samples).
640 *Identifying parallel patterns of allele frequency change and genome-wide evidence of trade-offs*
641 Statistical analysis of allele frequency data was conducted using R v. 3.5.6. We first
642 explored patterns of genomic divergence between samples as average F_{ST} across all segregating
643 sites. We compared F_{ST} between biological replicates (same replicate cage/collection time point,
644 different pool/extraction) to those values obtained for each replicate cage between its
645 generation 0 sample and all subsequent generation expansion samples. We quantified whether
646 evolutionary divergence increased throughout the course of expansion, and at what point it
647 exceeded the sources of biological noise impacting our allele frequency estimates, using a linear
648 regression.
649 We next explored whether increasing differentiation through time was underpinned by
650 parallel allele frequency shifts across replicates. Specifically, we used our pairwise divergence
651 values (i.e., F_{ST} between samples) to create multi-dimensional scaling (MDS) plots, in which

652 divergence between samples is represented as distance between points in a 2-D plane (*cmdscale*
653 function in *stats* package R). If the observed evolutionary change across replicates was
654 dominated by parallel responses to shifting population densities, then the segregation of
655 samples across the 2-D plane should, in part, correspond to the generation from which samples
656 were derived. This analysis was conducted on mean, genome-wide F_{st} values, as well as F_{st}
657 values computed separately for SNPs on each chromosomal arm. To quantify trends visualized
658 using MDS, we translated the coordinates for each cage such that the centroid of all generation 0
659 samples was centered at the origin and then projected all points onto a single axis which was
660 constructed by fitting a simple linear regression model to samples from generations 0-4
661 (regressions were constructed separately for each replicate cage). The resulting axis represents
662 the primary axis of variation in the 2D plane during early expansion for each replicate (Fig. S5).
663 We hypothesized that if sustained, directional selection imposed by population expansion was a
664 primary driver of patterns in genomic variation, the samples from the remaining expansion
665 generations would continue to proceed along the established axis of variation in the same
666 direction. To evaluate the degree of concordance of early and late expansion generation samples
667 we computed Pearson correlations between collection time and position along this axis. The
668 significance of these correlations was determined via permutations of sample collection time
669 point (N = 100 permutations). We conducted this analysis across all genome-wide SNPs, as well
670 as separately for SNPs on each chromosomal arm. Finally, to disentangle whether differences in
671 dynamics observed among chromosomal arms reflected true systematic differences in allele
672 frequency behavior, as opposed technical artifacts driven by differences in the number of SNPs
673 available for analysis across arms, we re-conducted this analysis using randomly sampled
674 subsets of SNPs matching that present on each arm.
675 We quantified the extent to which individual SNPs exhibited parallel movement across
676 cages and throughout expansion by fitting a generalized linear model to allele frequencies
677 (formula: allele frequency ~ expansion generation; *glm* function in base R) (Wiberg et al., 2017).
678 Allele frequencies were weighted by the total number of chromosomes sequenced (N = 200) and
679 depth per sample (Tilk et al., 2019). This model assessed the significance of the linear
680 relationship between allele frequency and generation of sampling across all cages, using a
681 quasibinomial error model to reduce false positive associations (Machado et al., 2021; Rudman
682 et al., 2022; Wiberg et al., 2017). While an association between allele frequency and sampling
683 timepoint within a single cage may represent either drift or selection, a significant association
684 across all four replicate cages indicates allele frequency trajectories that are both predictable
685 over time and parallel across populations. In this case, selection (or linked selection) is the more
686 parsimonious explanation. P-values were adjusted using the Benjamini-Hochberg false
687 discovery rate (FDR) correction (*p.adjust* package in base R). We considered a SNP significant if

688 it exhibited an FDR < 0.01 and effect size > 2%. We further validated the parallelism inferred by
689 the GLM by implementing a leave-one-out cross validation. Specifically, we iteratively
690 identified sets of parallel SNPs (FDR < 0.01 and effect size > 2%) across expansion samples
691 using a GLM and allele frequency data from three of the four replicate cages. We then
692 quantified the frequency shifts of the favored allele at significant sites in the left-out cage
693 between generation 0 and 9 of expansion. For sets of parallel SNPs identified via each iteration
694 of the leave-one-out validation, we matched each parallel SNP to a control SNP based on
695 chromosomal arm, starting frequency (within 5% of generation 0 frequency), inversion status,
696 and recombination rate. We compared the distribution of allele frequency shifts at parallel vs.
697 matched control sites (using a two-tailed, paired t-test) for each left out cage to infer if the
698 magnitude of allele frequency change exceeded background allele frequency movement, and
699 whether the dominant direction of allele frequency change was in a direction concordant with
700 the three training cages. We conducted this analysis for SNPs identified genome-wide, as well
701 as separately for each chromosomal arm.
702 *Quantifying evidence of fecundity and desiccation tolerance trade-offs*
703 We next used samples collected throughout truncation, during which patterns of
704 survival and selection were most likely underpinned by differences in desiccation resistance
705 among genotypes, to quantify the presence of fitness-tradeoffs at those alleles systematically
706 favored during expansion. First, we re-conducted our MDS analysis of pairwise divergence
707 values, this time including all samples collected across both phases of the experiment. While
708 general qualitative inference may be obtained from the visualization of this analysis, we
709 explicitly quantified the relative movement of expansion and truncation samples across this 2D
710 plane to provide a more rigorous investigation into the relative direction of allele frequency
711 movement across phases. Specifically, as above, we translated MDS coordinates for each cage
712 such that the centroid of all hour 0 truncation samples was centered at the origin, and then
713 projected onto a single axis which, as above, was constructed by fitting a simple linear
714 regression model to samples from expansion generations 0-4. We hypothesized that if our
715 contrasting reproduction/stress-tolerance selection environments were inducing genome-wide
716 reversions in allele frequency movement, then the projection of samples collected throughout
717 truncation would regress in the opposite direction as that observed for the expansion samples.
718 The degree of concordance/discordance for truncation samples were quantified as the Pearson
719 Correlation between collection time and position along this axis, and the significance of these
720 correlations was determined via permutations of sample collection time point (N = 100
721 permutations). This analysis was also conducted both genome-wide and separately for each
722 chromosomal arm and, as above, we used genome-wide subsampling to infer whether variation
723 in dynamics among chromosomal arms was a technical artifact.

724 Finally, we aimed to corroborate patterns observed in the dimensionality reduction of
725 genome and chromosome-wide F_{ST} values described above by accruing additional evidence of
726 genome-wide trade-offs using allele frequency trajectories. We first isolated those SNPs with
727 strong evidence of linkage to a selected locus throughout expansion (GLM FDR < 0.01 and allele
728 frequency shift > 2%). We then quantified the behavior of the rising allele at each SNP
729 throughout the progression of truncation, and evaluated whether these alleles were more likely
730 to exhibit a reversion in trajectory direction, or continue in the same direction, using a Chi-
731 squared test and set of control SNPs (matched on chromosome, starting frequency,
732 recombination rate, and inversion status). We further assessed if and how the results of this
733 analysis varied when only evaluating trajectories of expansion-identified SNPs that also
734 exhibited independent evidence of linkage to a selected locus (GLM FDR < 0.05 and allele
735 frequency shift > 1%) during truncation. Finally, we further quantified the distribution of
736 expansion-identified SNPs, genome-wide and per chromosomal arm, using empirical
737 cumulative distribution functions (eCDF). The eCDFs for SNPs with sustained directional
738 movement across treatments and evidence of fluctuating selection were evaluated
739 independently via comparison to eCDFs generated via a set of matched control SNPs, and using
740 a Kolmorgorov-Smirnov test (*stats* package in R).
741 *Assessing the role of inversions in fitness trade-offs*
742 From the known cosmopolitan inversions found in the DGRP lines (Huang et al., 2014),
743 we analyzed those that occurred in at least 10 of our founding strains (i.e., > 4%) (Huang et al.,
744 2014). We used chromosome-level haplotype frequencies to compute the frequencies of each of
745 these inversions independently during expansion and truncation. Next, we regressed inversion
746 frequencies through time using a generalized linear model (logistic link function, and
747 quasibinomial error variance) to classify inversions moving systematically across replicates
748 throughout each phase (Benjamini-Hochberg corrected P-value < 0.1). For those inversions
749 displaying significant frequency change across both expansion and truncation, we characterized
750 those that exhibited thus fluctuating selection and trade-offs (i.e. switched directions) across
751 phases.
752 We next aimed to quantify the extent to which SNPs within, or in tight linkage of, of the
753 assayed inversions underpinned genome-wide signals of trade-offs quantified in our
754 experiment. We thus first generated a winnowed set of genome-wide SNPs, eliminating those
755 either within, or up to 100 Kb away from, inversion breakpoints. We then explored whether we
756 retained signals of parallel adaptation throughout expansion and trade-offs during truncaiton
757 using this inversion-free SNP panel and re-conducting our F_{ST}-based MDS analysis of
758 expansion and truncation samples (described in *Quantifying evidence of fecundity and desiccation*
759 *tolerance trade-offs*, above).

Quantifying the emergence of trade-offs during adaptation to natural environmental fluctuations

We next quantified whether alleles identified via selection under sustained population expansion in a laboratory setting can predict patterns of adaption and trade-offs in an outdoor environment. Specifically, we leveraged data from an independent study year when we monitored patterns of genomic variation in a genetically diverse, outbred population that was split into a series of large, replicate cages maintained in a controlled, indoor laboratory, as well as outdoor mesocosms exposed to natural environmental fluctuations. Allele frequency data for the outdoor mesocosms were previously described, analyzed, and reported in Bitter *et al.* (2024). Briefly, the outdoor mesocosms were located in Philadelphia, Pennsylvania and consisted of twelve, replicate 2 m^3 cages, each consisting of a single dwarf peach tree and exposed to natural environmental fluctuations. The paired, indoor cage study (not reported or analyzed by Bitter *et al.* (2024)) consisted of ten, replicate ~0.5 m^3 cages housed in a temperature-controlled laboratory at the University of Pennsylvania.

The replicate cages for both the outdoor mesocosms and indoor cage study were seeded with a genetically diverse, outbred population, derived from a panel of 76 inbred strains originally collected wild from Linvilla Orchards, Media, PA (Supplementary Data File 2). Constat food was supplied to the replicates within each environment, whereby four hundred ml of Drosophila media ('Spradling cornmeal recipe') was provided in 900 cm^3 aluminum loaf pans within each cage three times per week. These pans provided the only source of food and egg laying substrate, and egg laying upon each loaf pan was carried out for two days, after which a new pan was added, and the original pan was covered with a mesh lid to prevent any further laying. The lids were removed after eclosure was first observed, causing each replicate to experience a near continual input of new flies that evolved with overlapping generations. The census size of the adult population in the outdoor mesocosms were estimated five times throughout the progression of the experiment (19 July, 5 August, 20 August, 17 September, and 20 October) (Bitter et al., 2024), while the final census in the indoor cages were estimated at the end of the monitoring period via collection and volumetric quantification of all flies remaining in each replicate. The outdoor mesocosms were sampled to quantify patterns of genomic variation weekly for 9 weeks (13 July – 7 September), after which samples were collected on 21 September, 20 October, and following the first freeze and population crash on 20 December (12 total time points). The indoor cages were sampled at the first, second, eighth, and eleventh time points. The overlapping monitoring period of the outdoor and indoor cages encompassed the rapid population expansion and ultimate stabilization of cage densities as the replicates in each environment presumably reached carrying capacity (Fig S11) (Bitter et al., 2024). The selective landscape experienced during this shared monitoring period probably mirrors that experienced under the sustained population expansion imposed by population expansion portion of the first

796 experiment of this study, described above. The notable differences between these experiments,
797 however, is that the first experiment increased food availability as a function of population
798 density throughout expansion, while our latter experiment maintained a constant food
799 substrate throughout the study period. Thus, this paired, indoor-outdoor study likely also
800 imposed selection on traits impacted by density regulation (e.g., larval competition). Analogous
801 to the truncation portion of the first experiment, the final collection interval of the outdoor
802 mesocosm study (time point 11->12) encompassed the onset of winter, during which time a
803 total crash of the adult populations in the cages was observed. Selection during this phase of the
804 experiment was thus hypothesized to favor increased in stress tolerance traits associated with
805 the deteriorating abiotic conditions.
806 Methods for sampling flies for sequencing from the outdoor mesocosms and indoor
807 cages were similar to those described above: eggs were collected overnight directly from each
808 replicate cage, and larval development was carried out in the indoor environment where eggs
809 developed and eclosed to F1 adults in 30 cm^3 cages. A random set of 100 females were sampled
810 from each cage 3-5 days post-eclosure and preserved in 99% ethanol at -20° C (Bitter et al., 2024).
811 Genomic DNA was extracted from pools of flies for each replicate and time point using the
812 Monarch Genomic DNA Purification Kit (New England Biolabs). Libraries were nonstructured
813 using the Illumina DNA Prep Tagmentation Kit and all samples were sequenced on Illumina
814 Novaseq 6000 flow cells using 150 bp, paired end reads. Raw sequencing reads from each
815 sample were trimmed of adapter sequences and bases with quality score < 20, and aligned to
816 the *Drosophila melanogaster* v5.39 reference genome using bwa and default parameters(Li and
817 Durbin, 2009). Aligned reads were deduplicated using Picard tools
818 (http://broadinstitute.github.io/picard/) and the final set of reads for each sample was down-
819 sampled to obtain an equivalent, genome-wide coverage of 8x across all samples (>100x
820 effective coverage) (Bitter et al., 2024; Tilk et al., 2019). Haplotype informed allele frequencies
821 from reads from each replicate and time point were then generated using the local inference
822 pipeline described above (see *Allele Frequency Calculation*) (Kessner et al., 2013; Tilk et al., 2019).
823 The final set of allele frequencies only included those sites with an average minor allele
824 frequency > 0.02 in the baseline population, and present in at least one evolved sample at a
825 MAF > 0.01, ultimately yielding 1.9 M SNPs (Bitter et al., 2024).
826 We quantified the extent to which evolution in the outdoor environment is driven by the
827 selective pressures solely associated with increasing population density (e.g., selection for
828 increased fecundity, faster developmental rate, increased competitive ability). Specifically, we
829 identified alleles with systematic behavior independently in the indoor and outdoor cages using
830 GLM (FDR < 0.01; allele frequency change > 2%), and compared the observed overlap between
831 these lists using a Chi squared test and with null expectations generated via a set of matched

control SNP set. Next, we queried whether the dominant direction of selection throughout the shared monitoring period of the indoor and outdoor environment was consistent. Specifically, we quantified the mean frequency shift of the rising allele at SNPs identified in the indoor environment via GLM, in the outdoor cages during the same time interval. We determined whether the magnitude of frequency shifts exceeded background allele frequency movement expected via matched control SNPs, and whether the dominant direction was parallel or anti-parallel given the sign of observed median shift (analysis conducted both genome-wide and separately for each chromosomal arm using a paired t-test and sign test). Finally, to test whether the total population crash in the outdoor mesocosms elicited evidence of the trade-offs, we quantified the behavior of the indoor identified alleles throughout this period. Through this, we used a common set of alleles, determined as linked to an advantageous locus during increasing population density in a controlled, lab-based setting, to infer the presence of trade-offs during a bout of population expansion and collapse in a semi-natural setting.

Acknowledgements: We are grateful to members of the Petrov and Schmidt labs for discussion during experimental design, lab work, and data analysis. We thank our funding organizations: the National Science Foundation (NSF PRFB 2109407 to M.C.B.) and the National Institutes of Health (NIH 5R35GM118165-07 to D.A.P and NIH R01GM100366 and R01GM137430 to P.S.), as well as funding support from the Chan Zukerberg Biohub.

Author Contributions: The experiment was conceived by D.A.P, P.S, A.O.B., S.R., and M.C.B. The population expansion/truncation experimental evolution study was conducted by S.R., N.B., and P.S. The paired indoor and outdoor mesocosm study was conducted by M.C.B., S.B., H.O., and P.S. DNA extraction, library preparation, and sequencing was conducted by S.T., A.O.B., S.G., and M.C.B. Bioinformatic analysis and statistical analysis of genomic data was carried out by A.O.B., S.G., J.H., and M.C.B. M.C.B., S.G., D.A.P, and P.S. wrote the manuscript, with feedback from all authors.

Data availability: Sequencing data from the DGRP lines used in the population expansion/truncation experiment are publicly available at http://dgrp2.gnets.ncsu.edu/data.html. Haplotype-informed allele frequency estimates from evolved, outbred samples and used in statistical analysis will be available at upon article publication. Founder line sequences for the paired indoor/outdoor mesocosm study are available at NCBI Accession PRJNA722305. Outdoor mesocosm sequences generated via pooled sequencing for this experiment are available at NCBI accession PRJNA1031645 and alle frequency data is available at the following Dryad repository: https://doi.org/10.5061/dryad.xd2547dpv. Indoor sequences and allele frequency data will be available upon article publication.

Code availability: Code associated with all analyses conducted in this manuscript are publicly available at the following repository: https://github.com/MarkCBitter/Drosophila-fitness-trade-offs .

References

Band, H.T., Ives, P.T., 1961. Correlated changes in environment and lethal frequency in a natural population of drosophila melanogaster. Proceedings of the National Academy of Sciences 47, 180–185. https://doi.org/10.1073/pnas.47.2.180

Behrman, E.L., Schmidt, P., 2022. How predictable is rapid evolution? https://doi.org/10.1101/2022.10.27.514123

Behrman, E.L., Watson, S.S., O'Brien, K.R., Heschel, M.S., Schmidt, P.S., 2015. Seasonal variation in life history traits in two Drosophila species. Journal of Evolutionary Biology 28, 1691–1704. https://doi.org/10.1111/jeb.12690

Berdan, E.L., Barton, N.H., Butlin, R., Charlesworth, B., Faria, R., Fragata, I., Gilbert, K.J., Jay, P., Kapun, M., Lotterhos, K.E., Mérot, C., Durmaz Mitchell, E., Pascual, M., Peichel, C.L., Rafajlović, M., Westram, A.M., Schaeffer, S.W., Johannesson, K., Flatt, T., 2023. How chromosomal inversions reorient the evolutionary process. J Evol Biol 36, 1761–1782. https://doi.org/10.1111/jeb.14242

Bergland, A.O., Behrman, E.L., O'Brien, K.R., Schmidt, P.S., Petrov, D.A., 2014. Genomic Evidence of Rapid and Stable Adaptive Oscillations over Seasonal Time Scales in Drosophila. PLOS Genetics 10, e1004775. https://doi.org/10.1371/journal.pgen.1004775

Bitter, M.C., Berardi, S., Oken, H., Huynh, A., Lappo, E., Schmidt, P., Petrov, D.A., 2024. Continuously fluctuating selection reveals fine granularity of adaptation. Nature 1–8. https://doi.org/10.1038/s41586-024-07834-x

Boor, G.K.H., Schultz, C.B., Crone, E.E., Morris, W.F., 2018. Mechanism matters: the cause of fluctuations in boom—bust populations governs optimal habitat restoration strategy. Ecological Applications 28, 356–372.

Boulétreau-Merle, J., Fouillet, P., Terrier, O., 1987. Seasonal variations and balanced polymorphisms in the reproductive potential of temperate D. Melanogaster populations.

Entomologia Experimentalis et Applicata 43, 39–48. https://doi.org/10.1111/j.1570-7458.1987.tb02200.x

Campbell-Staton, S.C., Arnold, B.J., Gonçalves, D., Granli, P., Poole, J., Long, R.A., Pringle, R.M., 2021. Ivory poaching and the rapid evolution of tusklessness in African elephants. Science 374, 483–487. https://doi.org/10.1126/science.abe7389

Campbell-Staton, S.C., Cheviron, Z.A., Rochette, N., Catchen, J., Losos, J.B., Edwards, S.V., 2017. Winter storms drive rapid phenotypic, regulatory, and genomic shifts in the green anole lizard. Science 357, 495–498. https://doi.org/10.1126/science.aam5512

Carroll, S.P., Hendry, A.P., Reznick, D.N., Fox, C.W., 2007. Evolution on ecological time-scales. Functional Ecology 21, 387–393. https://doi.org/10.1111/j.1365-2435.2007.01289.x

Charlesworth, B., 1994. Evolution in Age-Structured Populations, 2nd ed, Cambridge Studies in Mathematical Biology. Cambridge University Press, Cambridge. https://doi.org/10.1017/CBO9780511525711

Christie, M.R., McNickle, G.G., French, R.A., Blouin, M.S., 2018. Life history variation is maintained by fitness trade-offs and negative frequency-dependent selection. Proceedings of the National Academy of Sciences 115, 4441–4446. https://doi.org/10.1073/pnas.1801779115

Connallon, T., Chenoweth, S.F., 2019. Dominance reversals and the maintenance of genetic variation for fitness. PLOS Biology 17, e3000118. https://doi.org/10.1371/journal.pbio.3000118

Curtsinger, J.W., Service, P.M., Prout, T., 1994. Antagonistic Pleiotropy, Reversal of Dominance, and Genetic Polymorphism. The American Naturalist 144, 210–228. https://doi.org/10.1086/285671

Da Lage, J.-L., Capy, P., David, J.-R., 1989. Starvation and desiccation tolerance in *Drosophila melanogaster* adults: Effects of environmental temperature. Journal of Insect Physiology 35, 453–457. https://doi.org/10.1016/0022-1910(89)90051-6

de Bakker, P.I.W., Burtt, N.P., Graham, R.R., Guiducci, C., Yelensky, R., Drake, J.A., Bersaglieri, T., Penney, K.L., Butler, J., Young, S., Onofrio, R.C., Lyon, H.N., Stram, D.O., Haiman, C.A., Freedman, M.L., Zhu, X., Cooper, R., Groop, L., Kolonel, L.N., Henderson, B.E., Daly, M.J., Hirschhorn, J.N., Altshuler, D., 2006. Transferability of tag SNPs in genetic association studies in multiple populations. Nat Genet 38, 1298–1303. https://doi.org/10.1038/ng1899

Del Monte-Luna, P., Brook, B.W., Zetina-Rejón, M.J., Cruz-Escalona, V.H., 2004. The carrying capacity of ecosystems. Global Ecology and Biogeography 13, 485–495. https://doi.org/10.1111/j.1466-822X.2004.00131.x

Donihue, C.M., Herrel, A., Fabre, A.-C., Kamath, A., Geneva, A.J., Schoener, T.W., Kolbe, J.J., Losos, J.B., 2018. Hurricane-induced selection on the morphology of an island lizard. Nature 560, 88–91. https://doi.org/10.1038/s41586-018-0352-3

Durmaz, E., Benson, C., Kapun, M., Schmidt, P., Flatt, T., 2018. An inversion supergene in Drosophila underpins latitudinal clines in survival traits. Journal of Evolutionary Biology 31, 1354–1364. https://doi.org/10.1111/jeb.13310

Flatt, T., Amdam, G.V., Kirkwood, T.B.L., Omholt, S.W., 2013. Life-History Evolution and the Polyphenic Regulation of Somatic Maintenance and Survival. The Quarterly Review of Biology 88, 185–218. https://doi.org/10.1086/671484

Gleason, J.M., Roy, P.R., Everman, E.R., Gleason, T.C., Morgan, T.J., 2019. Phenology of Drosophila species across a temperate growing season and implications for behavior. PLOS ONE 14, e0216601. https://doi.org/10.1371/journal.pone.0216601

Grant, P.R., Abbott, I., Schluter, D., Curry, R.L., Abbott, L.K., 1985. Variation in the size and shape of Darwin's finches. Biological Journal of the Linnean Society 25, 1–39. https://doi.org/10.1111/j.1095-8312.1985.tb00384.x

Hendry, A.P., 2016. Eco-evolutionary Dynamics. Princeton University Press. https://doi.org/10.1515/9781400883080

Hoffmann, A A, Parsons, P.A., 1989. Selection for increased desiccation resistance in Drosophila melanogaster: additive genetic control and correlated responses for other stresses. Genetics 122, 837–845. https://doi.org/10.1093/genetics/122.4.837

Hoffmann, Ary A., Parsons, P.A., 1989. An integrated approach to environmental stress tolerance and life-history variation: desiccation tolerance in Drosophila. Biological Journal of the Linnean Society 37, 117–136. https://doi.org/10.1111/j.1095-8312.1989.tb02098.x

Huang, W., Massouras, A., Inoue, Y., Peiffer, J., Ràmia, M., Tarone, A.M., Turlapati, L., Zichner, T., Zhu, D., Lyman, R.F., Magwire, M.M., Blankenburg, K., Carbone, M.A., Chang, K., Ellis, L.L., Fernandez, S., Han, Y., Highnam, G., Hjelmen, C.E., Jack, J.R., Javaid, M., Jayaseelan, J., Kalra, D., Lee, S., Lewis, L., Munidasa, M., Ongeri, F., Patel, S., Perales, L., Perez, A., Pu, L., Rollmann, S.M., Ruth, R., Saada, N., Warner, C., Williams, A., Wu, Y.-Q., Yamamoto, A., Zhang, Y., Zhu, Y., Anholt, R.R.H., Korbel, J.O., Mittelman, D., Muzny, D.M., Gibbs, R.A., Barbadilla, A., Johnston, J.S., Stone, E.A., Richards, S., Deplancke, B., Mackay, T.F.C., 2014. Natural variation in genome architecture among 205 Drosophila melanogaster Genetic Reference Panel lines. Genome Res. 24, 1193–1208. https://doi.org/10.1101/gr.171546.113

Ives, P.T., 1945. THE GENETIC STRUCTURE OF AMERICAN POPULATIONS OF DROSOPHILA MELANOGASTER. Genetics 30, 167–196. https://doi.org/10.1093/genetics/30.2.167

Kapun, M., Fabian, D.K., Goudet, J., Flatt, T., 2016. Genomic Evidence for Adaptive Inversion Clines in Drosophila melanogaster. Molecular Biology and Evolution 33, 1317–1336. https://doi.org/10.1093/molbev/msw016

Kapun, M., Mitchell, E.D., Kawecki, T.J., Schmidt, P., Flatt, T., 2023. An Ancestral Balanced Inversion Polymorphism Confers Global Adaptation. Molecular Biology and Evolution 40, msad118. https://doi.org/10.1093/molbev/msad118

Kendall, B.E., Briggs, C.J., Murdoch, W.W., Turchin, P., Ellner, S.P., McCauley, E., Nisbet, R.M., Wood, S.N., 1999. Why Do Populations Cycle? A Synthesis of Statistical and Mechanistic Modeling Approaches. Ecology 80, 1789–1805. https://doi.org/10.1890/0012-9658(1999)080[1789:WDPCAS]2.0.CO;2

Kessner, D., Turner, T.L., Novembre, J., 2013. Maximum Likelihood Estimation of Frequencies of Known Haplotypes from Pooled Sequence Data. Mol Biol Evol 30, 1145–1158. https://doi.org/10.1093/molbev/mst016

Kirkpatrick, M., 2010. How and Why Chromosome Inversions Evolve. PLOS Biology 8, e1000501. https://doi.org/10.1371/journal.pbio.1000501

Kirkpatrick, M., Barton, N., 2006. Chromosome Inversions, Local Adaptation and Speciation. Genetics 173, 419–434. https://doi.org/10.1534/genetics.105.047985

Li, H., Durbin, R., 2009. Fast and accurate short read alignment with Burrows–Wheeler transform. Bioinformatics 25, 1754–1760. https://doi.org/10.1093/bioinformatics/btp324

Machado, H.E., Bergland, A.O., Taylor, R., Tilk, S., Behrman, E., Dyer, K., Fabian, D.K., Flatt, T., González, J., Karasov, T.L., Kim, B., Kozeretska, I., Lazzaro, B.P., Merritt, T.J., Pool, J.E., O'Brien, K., Rajpurohit, S., Roy, P.R., Schaeffer, S.W., Serga, S., Schmidt, P., Petrov, D.A., 2021. Broad geographic sampling reveals the shared basis and environmental correlates of seasonal adaptation in Drosophila. eLife 10, e67577. https://doi.org/10.7554/eLife.67577

Martinez, K.L., Klein, A., Martin, J.R., Sampson, C.U., Giles, J.B., Beck, M.L., Bhakta, K., Quatraro, G., Farol, J., Karnes, J.H., 2024. Disparities in ABO blood type determination across diverse ancestries: a systematic review and validation in the All of Us Research Program. Journal of the American Medical Informatics Association ocae161. https://doi.org/10.1093/jamia/ocae161

Mitchell-Olds, T., Willis, J.H., Goldstein, D.B., 2007. Which evolutionary processes influence natural genetic variation for phenotypic traits? Nat Rev Genet 8, 845–856. https://doi.org/10.1038/nrg2207

Nunez, J.C.B., Lenhart, B.A., Bangerter, A., Murray, C.S., Mazzeo, G.R., Yu, Y., Nystrom, T.L., Tern, C., Erickson, P.A., Bergland, A.O., 2024. A cosmopolitan inversion facilitates seasonal adaptation in overwintering Drosophila. Genetics 226, iyad207. https://doi.org/10.1093/genetics/iyad207

Rodríguez-Trelles, F., Tarrío, R., Santos, M., 2013. Genome-wide evolutionary response to a heat wave in Drosophila. Biol Lett 9, 20130228. https://doi.org/10.1098/rsbl.2013.0228

Roff, D.A., Fairbairn, D.J., 2007. The evolution of trade-offs: where are we? Journal of Evolutionary Biology 20, 433–447. https://doi.org/10.1111/j.1420-9101.2006.01255.x

Rose, M.R., 1982. Antagonistic pleiotropy, dominance, and genetic variation. Heredity 48, 63–78. https://doi.org/10.1038/hdy.1982.7

Rudman, S.M., Greenblum, S.I., Rajpurohit, S., Betancourt, N.J., Hanna, J., Tilk, S., Yokoyama, T., Petrov, D.A., Schmidt, P., 2022. Direct observation of adaptive tracking on ecological time scales in Drosophila. Science 375, eabj7484. https://doi.org/10.1126/science.abj7484

Schmidt, P.S., Paaby, A.B., Heschel, M.S., 2005. GENETIC VARIANCE FOR DIAPAUSE EXPRESSION AND ASSOCIATED LIFE HISTORIES IN DROSOPHILA MELANOGASTER. Evolution 59, 2616–2625. https://doi.org/10.1111/j.0014-3820.2005.tb00974.x

Schou, M.F., Engelbrecht, A., Brand, Z., Svensson, E.I., Cloete, S., Cornwallis, C.K., 2022. Evolutionary trade-offs between heat and cold tolerance limit responses to fluctuating climates. Science Advances 8, eabn9580. https://doi.org/10.1126/sciadv.abn9580

Service, P.M., 1987. Physiological Mechanisms of Increased Stress Resistance in Drosophila melanogaster Selected for Postponed Senescence. Physiological Zoology 60, 321–326. https://doi.org/10.1086/physzool.60.3.30162285

Shoval, O., Sheftel, H., Shinar, G., Hart, Y., Ramote, O., Mayo, A., Dekel, E., Kavanagh, K., Alon, U., 2012. Evolutionary Trade-Offs, Pareto Optimality, and the Geometry of Phenotype Space. Science 336, 1157–1160. https://doi.org/10.1126/science.1217405

Stearns, S.C., 1989. Trade-Offs in Life-History Evolution. Functional Ecology 3, 259–268. https://doi.org/10.2307/2389364

Sturtevant, A.H., 1921. A Case of Rearrangement of Genes in Drosophila1. Proceedings of the National Academy of Sciences 7, 235–237. https://doi.org/10.1073/pnas.7.8.235

Sturtevant, A.H., Beadle, G.W., 1936. THE RELATIONS OF INVERSIONS IN THE X CHROMOSOME OF DROSOPHILA MELANOGASTER TO CROSSING OVER AND DISJUNCTION. Genetics 21, 554–604. https://doi.org/10.1093/genetics/21.5.554

Tataru, D., Leon, M.D., Dutton, S., Perez, F.M., Rendahl, A., Ferris, K.G., 2024. Fluctuating selection in a Monkeyflower hybrid zone. https://doi.org/10.1101/2024.06.14.599085

Tilk, S., Bergland, A., Goodman, A., Schmidt, P., Petrov, D., Greenblum, S., 2019. Accurate Allele Frequencies from Ultra-low Coverage Pool-Seq Samples in Evolve-and-Resequence Experiments. G3 (Bethesda) 9, 4159–4168. https://doi.org/10.1534/g3.119.400755

Troth, A., Puzey, J.R., Kim, R.S., Willis, J.H., Kelly, J.K., 2018. Selective trade-offs maintain alleles underpinning complex trait variation in plants. Science 361, 475–478. https://doi.org/10.1126/science.aat5760

Turelli, M., Barton, N.H., 2004. Polygenic Variation Maintained by Balancing Selection: Pleiotropy, Sex-Dependent Allelic Effects and G × E Interactions. Genetics 166, 1053–1079. https://doi.org/10.1093/genetics/166.2.1053

Wiberg, R.A.W., Gaggiotti, O.E., Morrissey, M.B., Ritchie, M.G., 2017. Identifying consistent allele frequency differences in studies of stratified populations. Methods in Ecology and Evolution 8, 1899–1909. https://doi.org/10.1111/2041-210X.12810

Wittmann, M.J., Bergland, A.O., Feldman, M.W., Schmidt, P.S., Petrov, D.A., 2017. Seasonally fluctuating selection can maintain polymorphism at many loci via segregation lift. Proceedings of the National Academy of Sciences 114, E9932–E9941. https://doi.org/10.1073/pnas.1702994114

Zera, A.J., Harshman, L.G., 2001. The Physiology of Life History Trade-Offs in Animals. Annual Review of Ecology, Evolution, and Systematics 32, 95–126. https://doi.org/10.1146/annurev.ecolsys.32.081501.114006

Supplementary information for Bitter *et al.* (2024)

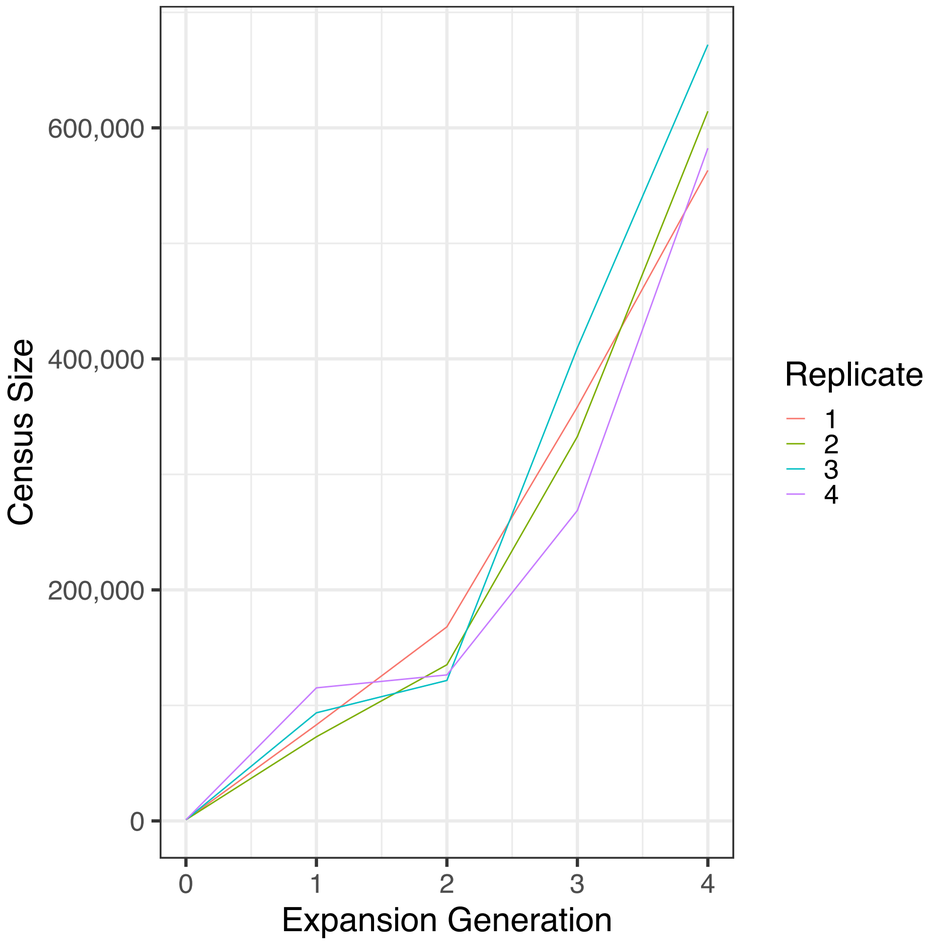

Figure S1. Census estimates of indoor replicate cages during the first four generations of population expansion.

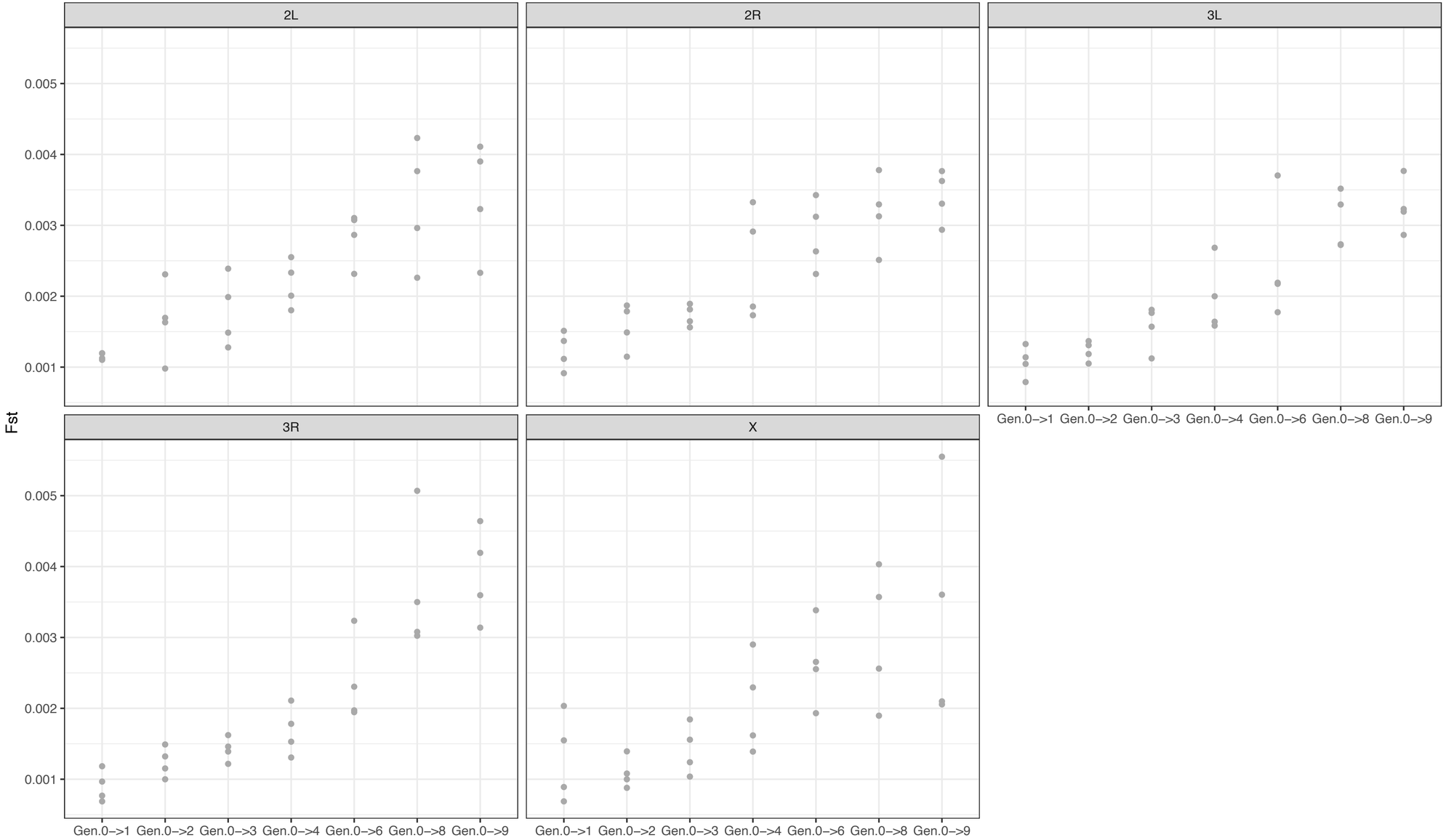

Figure S2. Evolution of allele frequencies across expansion generations | (A) Mean, genome-wide Fst between each evolved replicate and its generation 0 sample (Gen.0->n), segregated by chromosomal arm. Each grey dot corresponds to an individual replicate.

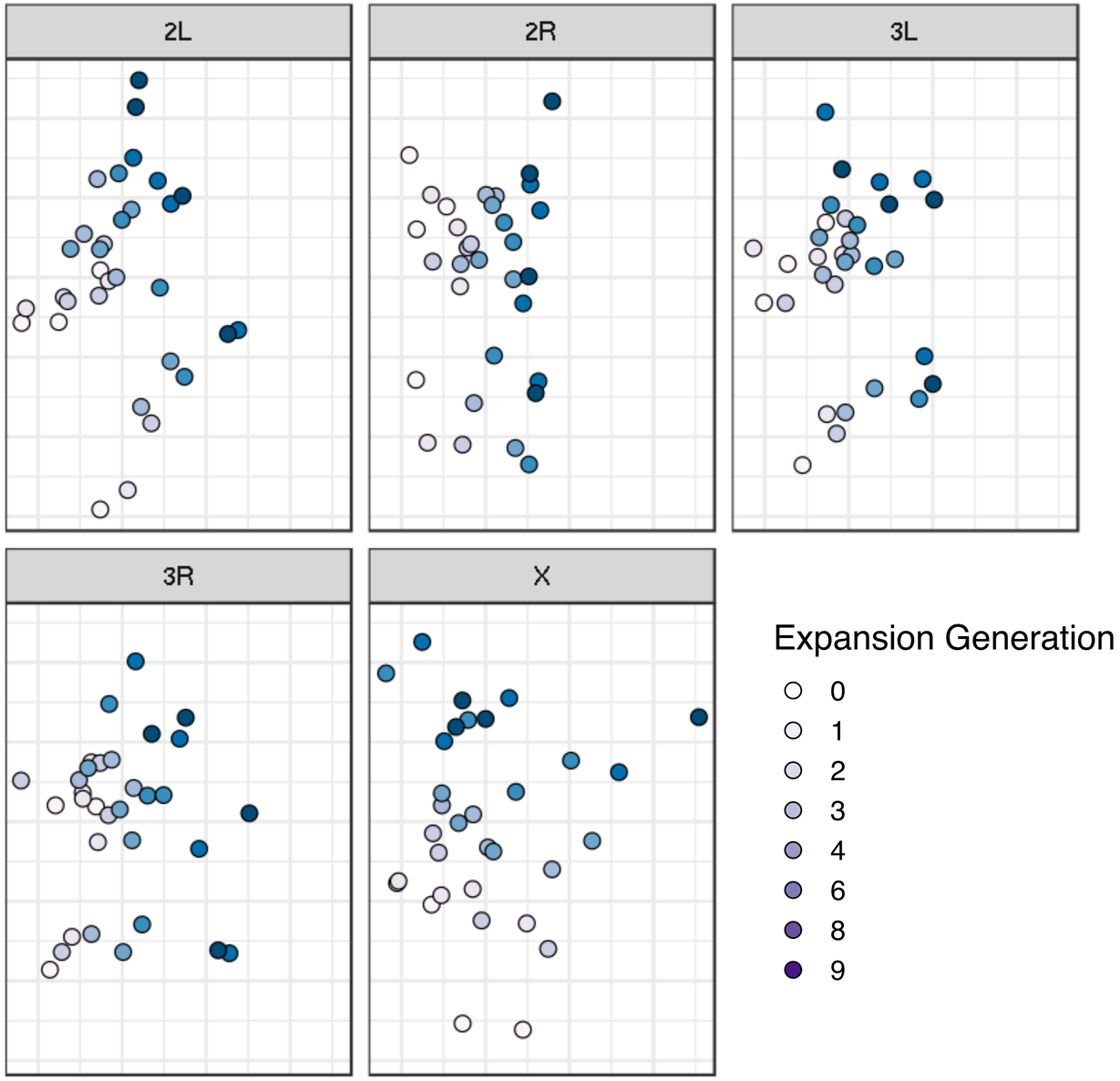

Figure S3. MDS of pairwise Fst values computed per chromosomal arm and and across all expansion samples. Point Color corresponds to sample expansion collection generation.

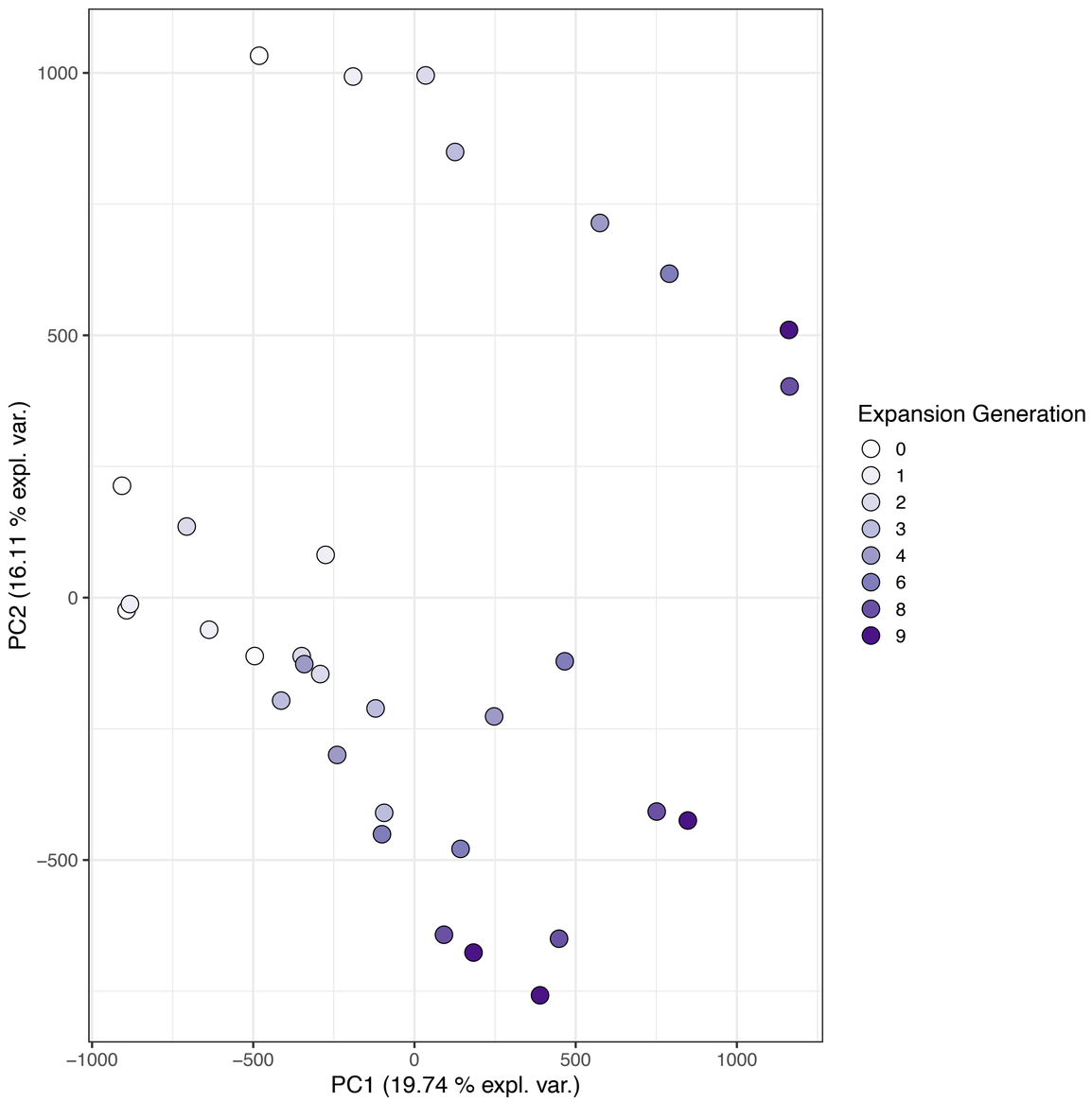

Figure S4. Principal component analysis of samples collected throughout expansion using allele frequency data across all 1.7 M SNPs. Samples are projected onto the first two principal components and colored in accordance with expansion generation collection time point.

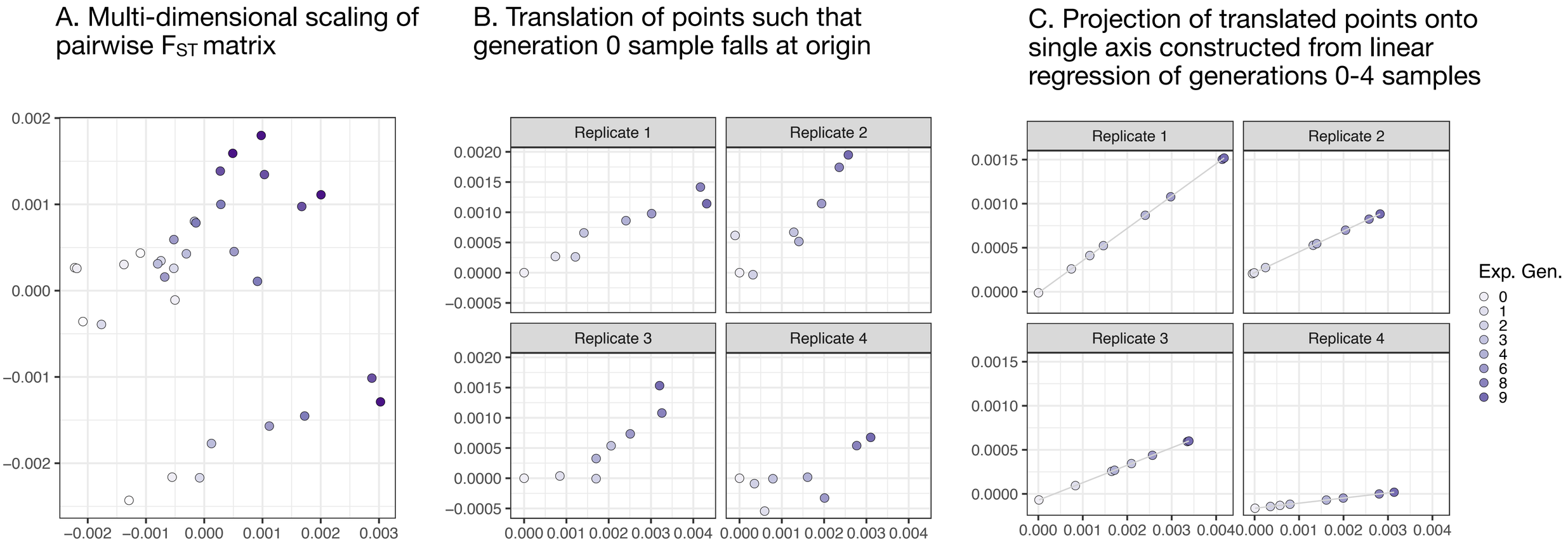

Figure S5. F_{ST}-based MDS analysis workflow. (A) Multi-dimensional scaling of expansion sample pairwise F_{ST} matrix as in main figure 2. (B) Translation of expansion points such that, for each replicate, the generation 0 sample falls at the plot origin. (C) Projection of translated points (B) onto a single axis constructed via a simple linear regression of generation 0-4 translated points.

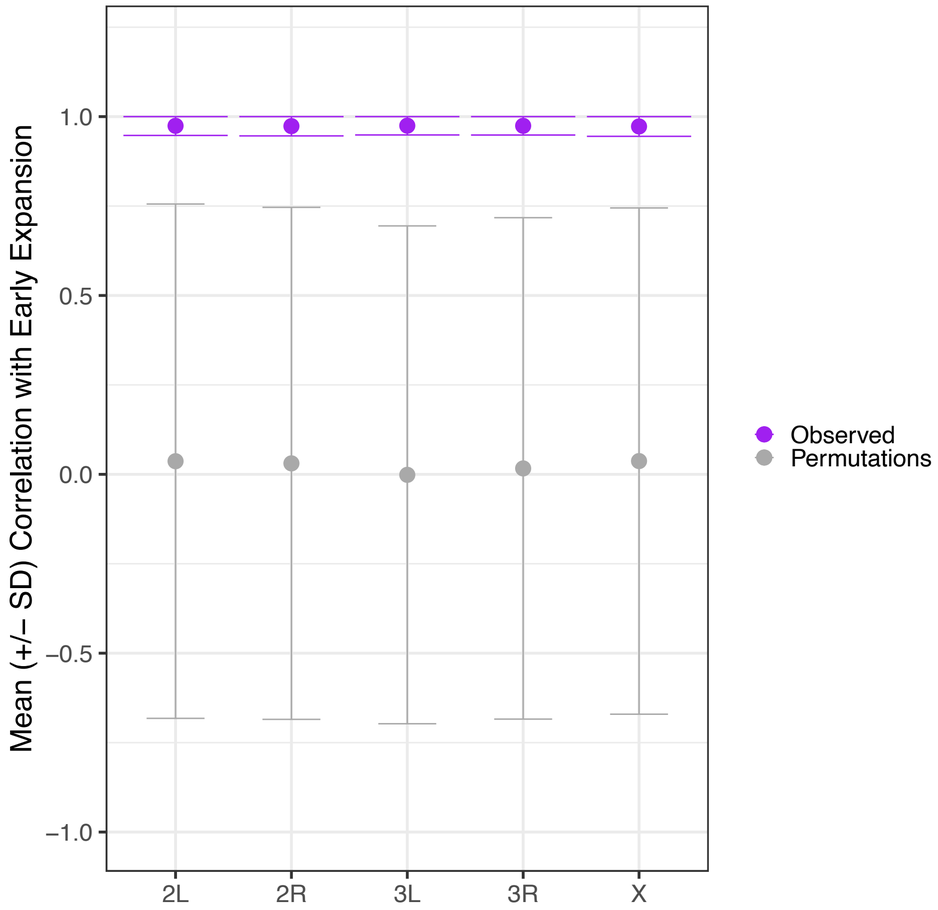

Figure S6. Average Pearson Correlation across replicates (+/- standard deviation) between sample expansion generation and distance along a one-dimensional axis constructed using F_{ST} MDS coordinates for early expansion (generation 0-4) samples. Purple points and error bars correspond to empirical values, while grey points and error bars correspond to values derived from empirical permutations (N = 100). Here, Fst values and MDS analysis was run on SNPs randomly sampled throughout the genome, matching the number of SNPs present on each chromosomal arm.

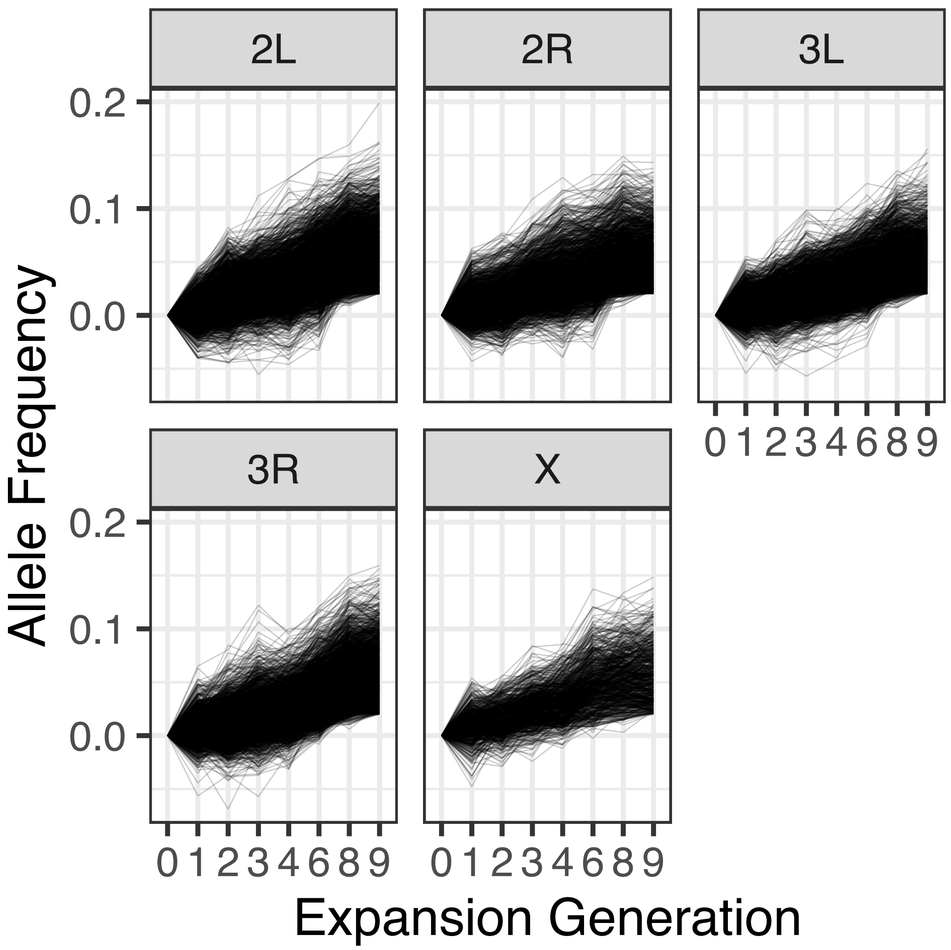

Figure S7. Trajectories of SNPs identified via GLM as exhibiting parallel frequency shifts across replicates throughout expansion (GLM FDR < 0.01 and effect size > 2%), segregated by chromosomal arm.

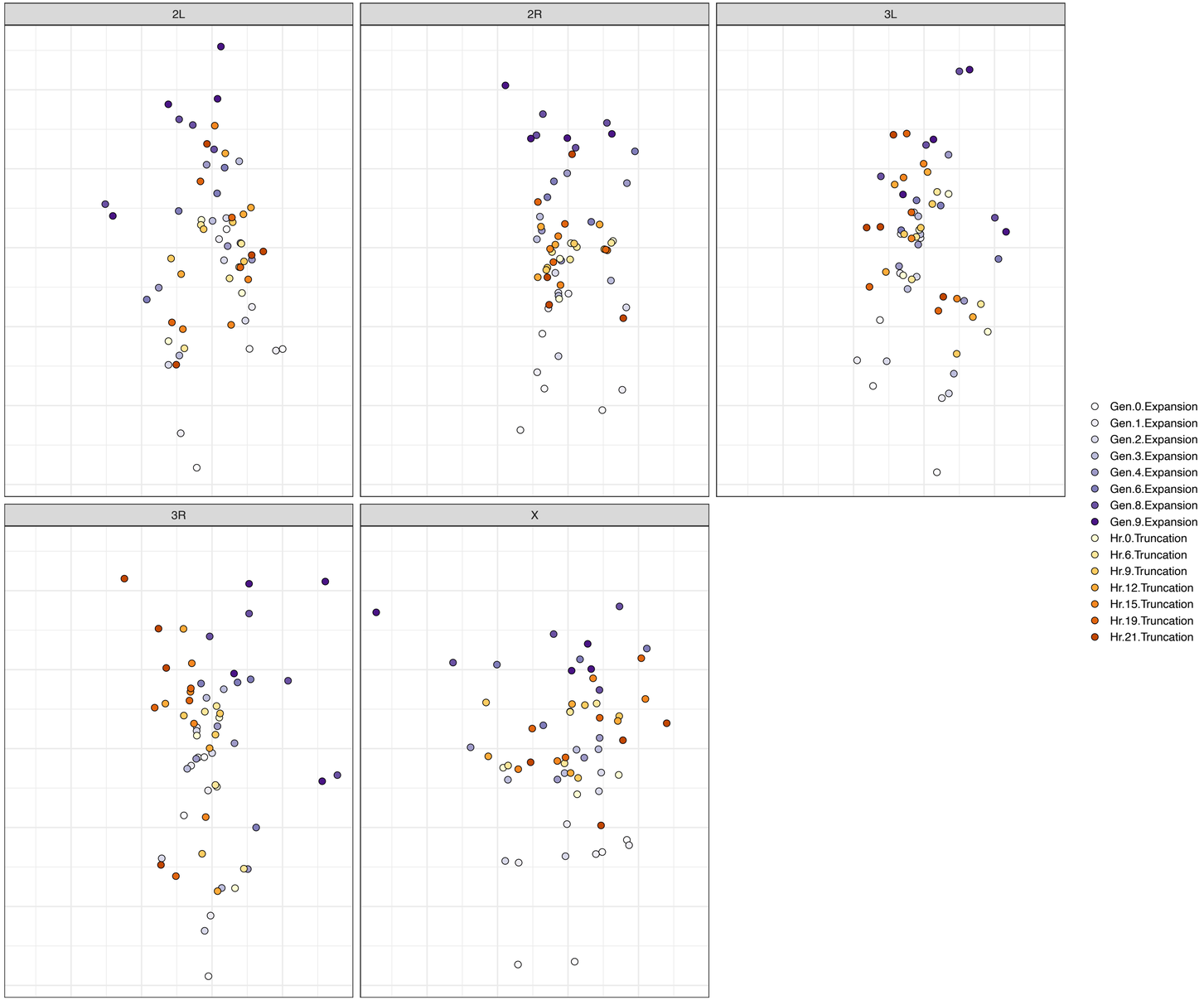

Figure S8. MDS of pairwise Fst values for each chromosomal arm and across all samples collected throughout expansion (purple-hue points) and truncation (orange-hue points). Points are shaded according to collection time point (darker hues indicate later expansion or truncation sampling generation/hour).

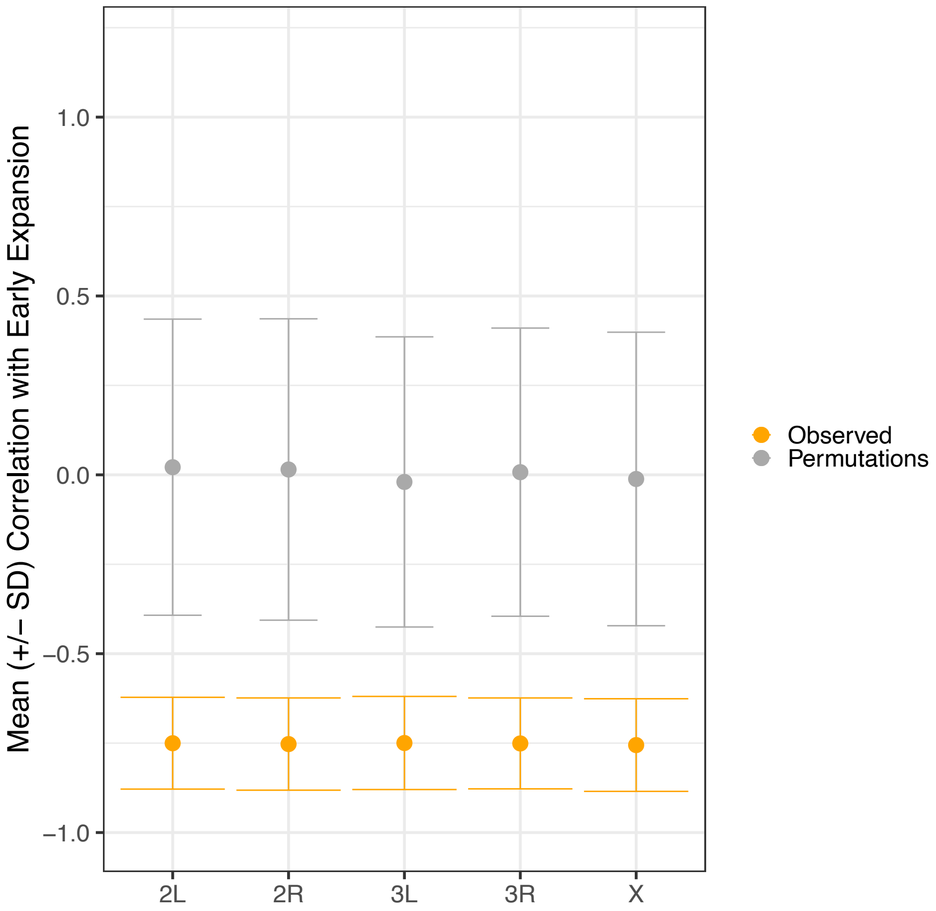

Figure S9. Average Pearson Correlation across replicates (+/- standard deviation) between sample truncation hour and distance along a one-dimensional axis constructed using F_{ST} MDS coordinates for early expansion (generation 0-4) samples. Orange points and error bars correspond to empirical values, while grey points and error bars correspond to values derived from empirical permutations (N = 100). Here, Fst values were derived from randomly sampled SNPs throughout the genome, matching the number of SNPs present on each chromosomal arm.

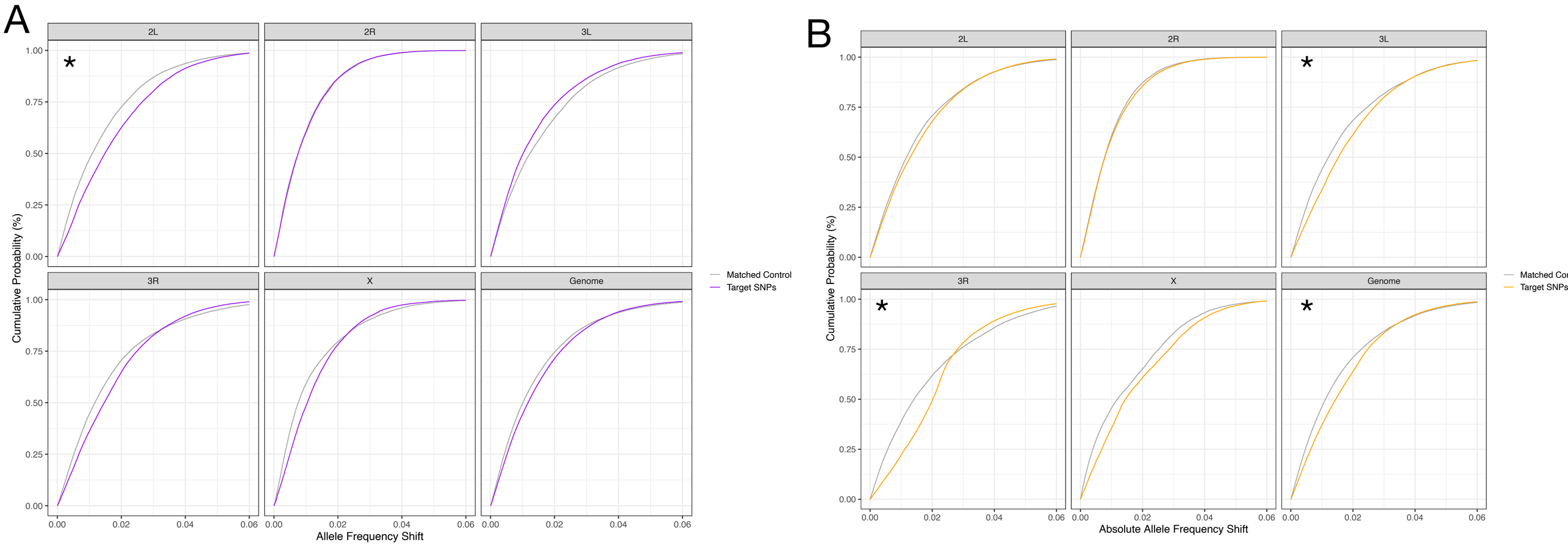

Figure S10. eCDFs of expansion-favored SNPs during truncation, segregated by those with sustained direction of movement (A) or reversals in direction (B). Asterisks correspond to instances in which the observed eCDF differed significantly from that generated via matched control SNPs (grey lines) (one-tailed Kolmogorov-Smirnov test, p-value < 0.05)

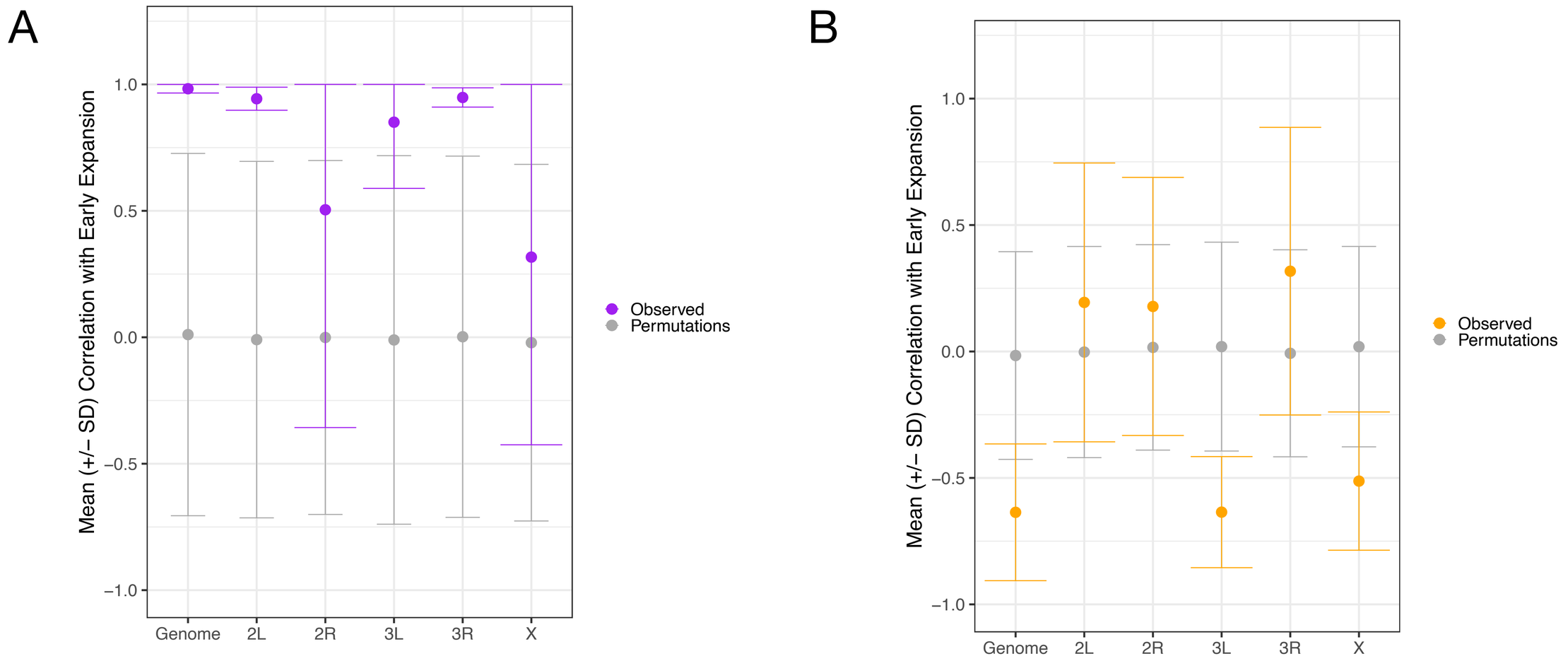

Figure S11. Average Pearson Correlation across replicates (+/- standard deviation) between sample expansion generation and distance along a one-dimensional axis constructed using F_{ST} MDS coordinates for early expansion (generation 0-4) samples. Purple points and error bars correspond to empirical values, while grey points and error bars correspond to values derived from empirical permutations (N = 100). Here, Fst values were derived from SNPs excluding those within, or up to 100 Kb away from, inversion breakpoints.

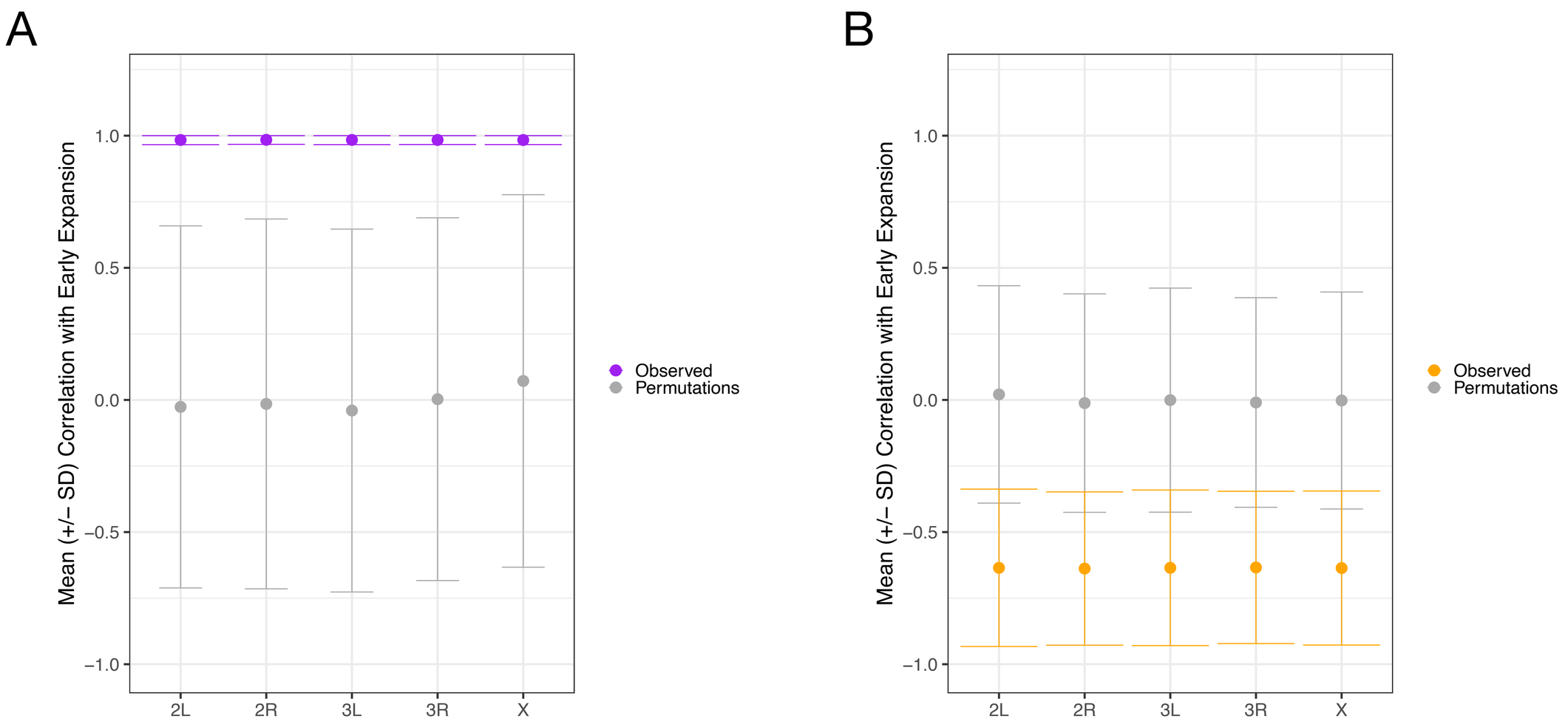

Figure S12. Average Pearson Correlation across replicates (+/- standard deviation) between sample expansion generation and distance along a one-dimensional axis constructed using F_{ST} MDS coordinates for early expansion (generation 0-4) samples. Purple points and error bars correspond to empirical values, while grey points and error bars correspond to values derived from empirical permutations (N = 100). Here, Fst values were derived from randomly sampled SNPs throughout the genome matched to the total number of SNPs present on each chromosomal arm and excluding those within, or up to 100 Kb away from, inversion breakpoints.

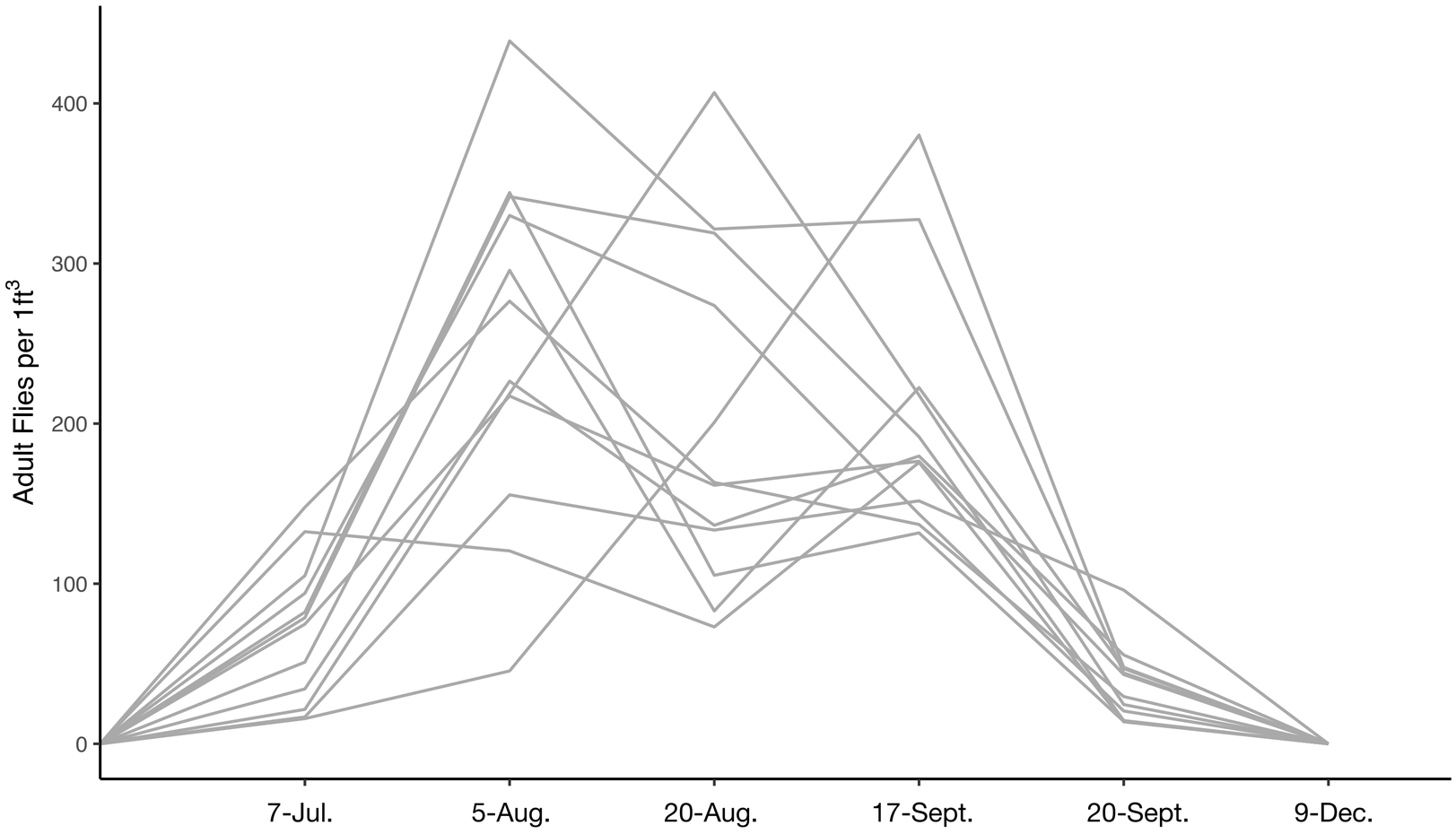

Figure S13. Census estimates of flies in the outdoor mesocosm experiment from 2021. Figure modified from Bitter *et al* . (2024).

Table S1 Statistics for projection of late expansion (generations 6-9) and truncation samples onto a one-dimensional axis constructed using F_{ST} MDS coordinates of early expansion (generation 0-4) samples. Correlation coefficients were computed between sample collection time point and distance along this axis for each cage, and reported are the median values across cage for each chromosomal arm, as well as when the analysis was run genome-wide. P-values were generated via comparison of each median correlation to a distribution generated via permutation of time point labels (N = 100 total permutations) .

Test Interval	Chromosome	Median Correlation	Permutation p-value
Late Expansion	2L	0.97213201683991	0.0337499999999999
Late Expansion	2R	-0.244238340356563	0.375
Late Expansion	3L	0.972604523272359	0.08875
Late Expansion	3R	0.988165487304083	0.05375
Late Expansion	X	0.315657111616651	0.425
Late Expansion	Genome	0.975609936558498	0.06875
Truncation	2L	-0.0443704606050802	0.43875
Truncation	2R	-0.317142428585079	0.23625
Truncation	3L	-0.578233415528078	0.06375
Truncation	3R	-0.862222504266232	0.005
Truncation	X	-0.504215848697299	0.13
Truncation	Genome	-0.753283710728129	0.01625

Table S2 Statistics for projection of late expansion (generations 6-9) and truncation samples onto a one-dimensional axis constructed using F_{ST} MDS coordinates of early expansion (generation 0-4) samples. Correlation coefficients were computed between sample collection time point and distance along this axis for each cage, and reported are the median values across cage for each chromosomal arm, as well as when the analysis was run genome-wide. P-values were generated via comparison of each median correlation to a distribution generated via permutation of time point labels (N = 100 total permutations). Here, Fst values and MDS analysis was run on SNPs randomly sampled throughout the genome, matching the number of SNPs present on each chromosomal arm.

Test Interval	Chromosome	Median Correlation	Permutation p-value
Late Expansion	2L	0.975716766359953	0.07375
Late Expansion	2R	0.974541408118333	0.075
Late Expansion	3L	0.975540423627953	0.01875
Late Expansion	3R	0.9752928069539	0.02625
Late Expansion	X	0.973467774354005	0.0600000000000001
Truncation	2L	-0.751876958283634	0.02
Truncation	2R	-0.753904647531668	0.01875
Truncation	3L	-0.7502678134965	0.04125
Truncation	3R	-0.750207616089703	0.025
Truncation	X	-0.756320833115252	0.0225

Table S3 Inversion Frequency Dynamics | GLM regression summary statistics of the expansion and truncation dynamics of four major cosmopolitan inversions segregating in our outbred population of DGRP lines. The FDR corrected p-value for each inversion during both phases of the experiment (expansion and truncation) are presented, alongside the mean inversion frequency shift in cases in which the GLM regression was significant.

Inversion	Selection Phase	FDR P-value	Frequency Shift
In(2L)t	Expansion	0.094*	-0.97%
In(2L)t	Truncation	0.426	Not significant
In(2R)NS	Expansion	<0.001**	-3.02%
In(2R)NS	Truncation	0.439	Not significant
In(3R)K	Expansion	<0.001**	1.65%
In(3R)K	Truncation	<0.001**	-1.35%
In(3R)Mo	Expansion	0.003**	-7.49%
In(3R)Mo	Truncation	0.017**	-1.73%
In(3R)P	Expansion	0.001**	1.17%
In(3R)P	Truncation	<0.001**	-1.21%

Table S4 Statistics for projection of late expansion (generations 6-9) and truncation samples onto a one-dimensional axis constructed using F_{ST} MDS coordinates of early expansion (generation 0-4) samples. Correlation coefficients were computed between sample collection time point and distance along this axis for each cage, and reported are the median values across cage for each chromosomal arm, as well as when the analysis was run genome-wide. P-values were generated via comparison of each median correlation to a distribution generated via permutation of time point labels (N = 100 total permutations). Here, Fst values and MDS analysis was run on a set of SNPs excluding those within, or up to 100 Kb away from, inversion breakpoints.

Test Interval	Chromosome	Median Correlation	Permutation p-value
Late Expansion	2L	0.941877272974043	0.15875
Late Expansion	2R	0.906664673672926	0.12875
Late Expansion	3L	0.972604523272357	0.0925
Late Expansion	3R	0.949409974764516	0.10375
Late Expansion	X	0.315657111616649	0.39
Late Expansion	Genome	0.988690601491595	0.0855
Truncation	2L	0.193910187619202	0.345
Truncation	2R	0.1106453838666	0.41375
Truncation	3L	-0.578233415528078	0.0775
Truncation	3R	0.516639815656395	0.10625
Truncation	X	-0.504215848697302	0.10125
Truncation	Genome	-0.660159220395907	0.047

Table S5 Statistics for projection of late expansion (generations 6-9) and truncation samples onto a one-dimensional axis constructed using F_{ST} MDS coordinates of early expansion (generation 0-4) samples. Correlation coefficients were computed between sample collection time point and distance along this axis for each cage, and reported are the median values across cage for each chromosomal arm, as well as when the analysis was run genome-wide. P-values were generated via comparison of each median correlation to a distribution generated via permutation of time point labels (N = 100 total permutations). Here, Fst values and MDS analysis was run on SNPs randomly sampled throughout the genome, matched to the number of SNPs present on each chromosomal arm, and excluding those within, or up to 100 Kb away from, inversion breakpoints.

Test Interval	Chromosome	Median Correlation	Permutation p-value
Late Expansion	2L	0.988413197497469	0.0525
Late Expansion	2R	0.989942495115707	0.05125
Late Expansion	3L	0.989390312932461	0.05
Late Expansion	3R	0.990068206319797	0.06375
Late Expansion	X	0.989855205403952	0.08125
Truncation	2L	-0.665094200789921	0.04375
Truncation	2R	-0.661142450550023	0.055
Truncation	3L	-0.660888966235905	0.0525
Truncation	3R	-0.653623292619365	0.03875
Truncation	X	-0.660601423436917	0.045

Table S6 Statistics for comparison of rising allele frequency shifts of indoor-identified SNPs in an outdoor mesocosm during population expansion and collapse. Target values (Mean.Target, Median.Target) indicate those derived from indoor-identified SNPs, while matched values indicate those derived from control SNPs. The distributions of target and matched sites were compared using both a two-tailed t-test and sign test. The resulting test statistics are provided.

Chromosome	Mean.Target	Median.Target	Mean.Matched	Median.Matched	t	FDR.t.test	FDR.sign.test	Test.Interval
2L	0.0319985981378007	3.038013e-02	0.00316831802589668	3.178635e-03	90.4650925090862	0.000000e+00	8.326673e-16	Expansion
2R	0.028969065444205	2.551098e-02	0.00115295987609255	1.615365e-03	66.0420368142833	0.000000e+00	8.326673e-16	Expansion
3L	0.0335003699797639	3.080976e-02	0.00286597441953921	3.928358e-03	90.8841932663739	0.000000e+00	8.326673e-16	Expansion
3R	0.0369291946950844	3.378144e-02	0.00264119051901511	3.484494e-03	129.54052005962	0.000000e+00	8.326673e-16	Expansion
X	0.0288667950506608	2.644817e-02	0.0025943771973813	3.045992e-03	60.462689719572	0.000000e+00	8.326673e-16	Expansion
Genome	0.0333054320018882	3.057965e-02	0.00260823894732216	3.234185e-03	199.627700493635	0.000000e+00	8.326673e-16	Expansion
2L	-0.00487214737932314	-4.692767e-03	-0.00104825093438945	-9.152650e-04	-19.5690789120401	2.356927e-84	7.180716e-52	Collapse
2R	0.000478905306333812	8.868033e-04	-0.000171925992292266	4.171333e-05	2.8948882077324	3.958655e-03	9.993639e-05	Collapse
3L	0.00187994456347232	1.696414e-03	-7.9971808333333e-05	2.173192e-04	8.39801534836484	5.830216e-17	1.057355e-15	Collapse
3R	-0.000895085879399349	-1.074300e-04	0.000631816786767623	6.350982e-04	-8.12116003302136	5.475990e-16	3.364728e-06	Collapse
X	-0.000821591180249633	4.711083e-05	-0.000622166078071464	3.165075e-04	-0.573004050626995	5.666659e-01	3.673839e-02	Collapse
Genome	-0.00109679281216485	-5.765000e-04	-0.000135973486759733	9.451667e-05	-9.42612164714719	4.364745e-21	2.861040e-08	Collapse

Table S7 Final fly census size in indoor cages from paired indoor-outdoor mesocosm study. Census sizes were estimated volumetrically using the total remaining flies at the final collection time point (each replicate was originally seeded with 1,000 total flies).

Replicate	Census estimate
1	67200
2	120000
3	83400
4	67800
5	90000
6	90600
7	97800
8	70200
9	69000
10	51600